EBioMedicine 72 (2021) 103617

Contents lists available at ScienceDirect

EBioMedicine

journal homepage: www.elsevier.com/locate/ebiom

Deiodinase-3 is a thyrostat to regulate podocyte homeostasis

Shivangi Agarwal[a,1], Kwi Hye Koh[a,1], Nicholas J. Tardi[a,1], Chuang Chen[a], Ranadheer Reddy Dande[a], Joao Pedro WerneckdeCastro[a,2], Yashwanth Reddy Sudhini[a], Cristina Luongo[b], Domenico Salvatore[b], Beata Samelko[a], Mehmet M. Altintas[a], Steve Mangos[a], Antonio Bianco[c], Jochen Reiser[a,*]

[a] Department of Internal Medicine, Rush University, Chicago, IL 60612
[b] Department of Public Health, University of Naples "Federico II," Naples, Italy
[c] Department of Medicine, University of Chicago, Chicago, IL 60637

ARTICLE INFO

Article History:
Received 17 June 2021
Revised 22 September 2021
Accepted 22 September 2021
Available online xxx

Keywords:
D3
podocytes
deiodinases
thyroid
integrin
kidney
Graves' disease

ABSTRACT

Background: Nephrotic syndrome (NS) is associated with kidney podocyte injury and may occur as part of thyroid autoimmunity such as Graves' disease. Therefore, the present study was designed to ascertain if and how podocytes respond to and regulate the input of biologically active thyroid hormone (TH), 3,5,3′-triiodothyronine (T3); and also to decipher the pathophysiological role of type 3 deiodinase (D3), a membrane-bound selenoenzyme that inactivates TH, in kidney disease.

Methods: To study D3 function in healthy and injured (PAN, puromycin aminonucleoside and LPS, Lipopolysaccharide-mediated) podocytes, immunofluorescence, qPCR and podocyte-specific D3 knockout mouse were used. Surface plasmon resonance (SPR), co-immunoprecipitation and Proximity Ligation Assay (PLA) were used for the interaction studies.

Findings: Healthy podocytes expressed D3 as the predominant deiodinase isoform. Upon podocyte injury, levels of *Dio3* transcript and D3 protein were dramatically reduced both *in vitro* and in the LPS mouse model of podocyte damage. D3 was no longer directed to the cell membrane, it accumulated in the Golgi and nucleus instead. Further, depleting D3 from the mouse podocytes resulted in foot process effacement and proteinuria. Treatment of mouse podocytes with T3 phenocopied the absence of D3 and elicited activation of $\alpha v\beta 3$ integrin signaling, which led to podocyte injury. We also confirmed presence of an active thyroid stimulating hormone receptor (TSH-R) on mouse podocytes, engagement and activation of which resulted in podocyte injury.

Interpretation: The study provided a mechanistic insight into how D3-$\alpha v\beta 3$ integrin interaction can minimize T3-dependent integrin activation, illustrating how D3 could act as a renoprotective thyrostat in podocytes. Further, injury caused by binding of TSH-R with TSH-R antibody, as found in patients with Graves' disease, explained a plausible link between thyroid disorder and NS.

Funding: This work was supported by American Thyroid Association (ATA-2018-050.R1).

1. Introduction

Podocytes, terminally differentiated epithelial cells within the kidney glomerulus, play an instrumental role in the ultrafiltration process. Malfunction of the glomerular filtration barrier (GFB) is generally attributed to podocyte injury [1]. Podocytes are metabolically active and demand a large energy supply, and evidence suggests a correlation between mitochondrial dysfunction and podocytopathy [2, 3]. Although podocytes were originally considered as mere structural components of the glomerulus, they have recently been shown to possess mechanisms that respond to both glomerular-derived and systemically circulating hormones and other humoral factors [4]. Here we explored a potential link between podocytes and thyroid

Abbreviations: D1, Type 1 iodothyronine selenodeiodinase; D2, Type 2 iodothyronine selenodeiodinase; D3, Type 3 iodothyronine selenodeiodinase; T4, Thyroxine; T3, 3,5,3′-triiodothyronine; T2, 3,3′-diiodothyronine; rT3, reverse-3,3′,5′-triiodothyronine; FSGS, focal segmental glomerulosclerosis; DN, diabetic nephropathy; CKD, chronic kidney disease; MCD, minimal change disease; GBM, glomerular basement membrane; PM, plasma membrane; Sec, selenocysteine; LPS, lipopolysaccharides; IOP, iopanoic acid; FP, foot process; PAN, puromycin aminonucleoside; TH, thyroid hormone or T3; NS, nephrotic syndrome, TSH-R, Thyroid stimulating hormone receptor

* Corresponding author at: 1717 W Congress Parkway, Rush University, Chicago, IL 60612.
E-mail address: jochen_reiser@rush.edu (J. Reiser).

[1] Authors contributed equally
[2] Present address: University of Miami, Florida 33124.

https://doi.org/10.1016/j.ebiom.2021.103617

Research in context

Thyroid hormones (TH) are circulating iodinated signaling molecules that orchestrate physiological and developmental processes in nearly all the cells. Deiodinase 3 (D3) is a membrane-bound catabolic enzyme that deactivates the bioactive TH, 3,5,3′-triiodothyronine (T3). Although, deiodinases-mediated regulation of TH activity has been studied extensively in several tissues, how their anomalous expression, function or regulation impacts renal physiology is poorly understood. Dysregulation of TH has been associated with glomerular diseases and renal complications, indicating an obvious crosstalk between thyroid and kidneys. Additionally, other evidences point towards an overlap between them; (a) Chronic kidney disease (CKD) has been characterized by a low T3 syndrome; (b) patients with thyroid cancer exhibit a genetic predisposition for the development of renal cell carcinomas (RCC), and vice versa; (c) Recommendation for thyroid gland assessment in subjects with idiopathic kidney disease (KD); (d) Drugs used to combat thyroid disorders or KDs display adverse effects on the other organ's functions. Despite this precedence, how TH signaling locally affects renal cells remained an under delved arena. Therefore, the present study was undertaken to bridge this chasm in our understanding of how these two organs function synergistically.

Added value of this study

We demonstrate that healthy podocytes express D3 isoform in abundance. However, when podocytes were injured, a dramatic reduction in the *Dio3* mRNA and protein levels was observed; accompanied by a loss of D3 activity. Concomitantly, translocation of D3 to the plasma membrane was compromised, which was instead found in nuclear and Golgi compartments. These effects were recapitulated *in vivo*. Lipopolysaccharide (LPS)-induced kidney injury mouse model exhibited a substantial decrease in the glomerular *Dio3* mRNA levels. Podocyte-specific D3 deletion led to severe proteinuria along with podocyte foot process effacement. Upon exposing mouse podocytes to excess T3, which mimics the absence of D3, we were able to activate the deleterious $\alpha v\beta 3$ integrin signaling pathway. Our findings thus identified that D3 dysfunction or down-regulation, defined by reduced T3 deactivating capacity, enhanced local thyroid hormone action in podocytes leading to an increased susceptibility to nephrotic injury via activation of integrin signaling cascade. Additionally, D3 was shown to interact directly with $\alpha v\beta 3$ integrin *in vitro* and in cells; probably as an alternative protective mechanism to block the integrin receptor from activation. To mechanistically couple thyroid hormone dysfunction with KDs, we also show that thyroid stimulating hormone receptor (TSH-R) is not only expressed but is functionally active on the surface of mouse podocytes; activation of which induces injury. This explains how nephrotic syndrome (NS) is associated with thyroid malfunction as seen in Graves' disease, an autoimmune disorder characterized by circulating antibodies directed against TSH-R.

Implications of all the available evidence

Our study unequivocally demonstrated a novel renoprotective role for D3 in podocytes and provided a missing link that integrated the thyroid-kidney axis. The study also provides a proof of concept that interjecting TH signaling in podocytes via deiodinases could be exploited as a potential therapeutic strategy to prevent or treat KDs. Further, down-regulation of D3 expression could be used as a sensor/biomarker for assessing the progression and severity of KDs. Our data also advises clinicians to monitor TH levels in patients with NS.

hormones (TH), which are circulating iodinated signaling molecules that regulate physiological and developmental processes in virtually all cells [5].

In support of this, dysregulation of TH in the kidney has been associated with glomerular diseases and other renal complications [6–9]. While hyperthyroidism has been associated with increased renal blood flow and absorption capacity, hypothyroidism can be associated with thickening of the glomerular basement membrane (GBM) and reduced filtration rate, indicating a distinct overlap between the proper functioning of the thyroid gland and health of kidneys [7]. Additionally, patients with Graves' disease, an autoimmune form of hyperthyroidism characterized by presence of thyroid stimulating autoantibodies directed against the thyroid stimulating hormone receptor (TSH-R) leading to receptor activation [10], exhibit membranous glomerulonephritis with nephrotic syndrome (NS) [11], and also some sporadic cases of membranoproliferative glomerulonephritis or minimal change disease have been reported [12]. On the other hand, hypothyroidism has been associated with NS, but only as a secondary outcome due to increased urinary loss of TH [13]. Since NS is more closely and causally linked with hyperthyroidism as its primary outcome, the present study was specifically designed to ascertain if and how podocytes respond to and regulate T3 input, the biologically active TH.

TH signaling can be locally regulated by deiodinases [14]. Thyroxine (T4) secreted by the thyroid gland is a prohormone with minimal activity and is converted to T3 via either type 1 or 2 iodothyronine deiodinases (D1/D2) in extrathyroidal tissues [15]. Alternatively, the levels of T3 are reduced by type 3 iodothyronine deiodinase (D3; encoded by *Dio3*), an enzyme that irreversibly converts T3 to, 3,3′-diiodothyronine (T2). D3 also converts T4 to reverse T3 (rT3), an inactive molecule, dampening TH signal [16, 17]. Thus, iodothyronine deiodinases can initiate or terminate thyroid hormone action locally, independent of changes in TH serum concentrations. Our study demonstrates that TH acts on podocytes via extranuclear non-canonical pathway. Accordingly, a podocyte-specific reduction in D3 activity locally enhanced TH signaling, increasing susceptibility to nephrotic injury.

2. Methods

2.1. Reagents

Lipopolysaccharide (LPS) was procured from *E. coli* O111:B4 (LPSEB; Invitrogen, tlrl-eblps), collagen I from rat tail (Gibco, #A10483), puromycin aminonucleoside (Sigma-Aldrich, #P7130), 3,5,3′-triiodo-L-thyronine sodium salt (Sigma-Aldrich, #T6397) and 3,3′,5,5′-Tetraiodothyroacetic acid abbreviated as Tetrac (Sigma-Aldrich, #T3787) and Cyclo [Arg-Gly-Asp-D-Phe-Val] peptide (Enzo Life Sciences, BML-AM100-0001). Alexa Fluor™ 488 Phalloidin was from Invitrogen (A12379). Anti-TSH Receptor (TSH-R) (extracellular) Antibody (# ATR-006; RRID:AB_2341080) was from Alomone Labs. Recombinant mouse TSH alpha/beta Heterodimer protein (# 8885-TH-010/CF) was from R&D Systems. Mouse C57 thyroid tissue lysate was from Zyagen Labs (Fisher Scientific, #50-171-8790).

2.2. Cell culture

Immortalized human podocytes were cultured at 37°C for 10–14 days for full differentiation as previously described [18]. The culture medium was RPMI-1640 medium (Gibco, 11875) enriched with 10% fetal bovine serum (FBS; Denville Scientific, FB5001-H), insulin, transferrin and selenium (10.0 μg/ml, 5.5 μg/ml, and 6.7 ng/ml, respectively) supplement (Gibco, 41400045), 100 U/ml penicillin, and 100 μg/ml streptomycin (Gibco, A15140). Immortalized mouse podocytes were cultured as described [19]. All tissue culture flasks were coated with collagen I prior to seeding mouse

podocytes. Briefly, cells were cultured at 33°C for proliferation in RPMI-1640 medium containing 10% FBS, 100 U/ml penicillin, and 100 μg/ml streptomycin supplemented with mouse recombinant interferon-γ (Cell Sciences, CR2041), at an initial concentration of 50 U/ml for the first 2 passages and then 20 U/ml for continuous passages. For differentiation, cells were thermoshifted to 37°C for 10–14 days without interferon-γ. Prior to drug treatment, podocytes were serum starved using charcoal stripped sterile FBS (Millipore, Sigma).

2.3. Reverse transcription and quantitative polymerase chain reaction (qPCR) assays

Total RNA was isolated from cultured cells grown in three independent wells (biological replicates) using Trizol reagent (Invitrogen) or RNAeasy Mini Kit (Qiagen) following the manufacturer's instructions. The concentration and quality of RNA was determined spectrophotometrically by measuring absorbance values at 260 nm (A260) and 280 nm (A280) and evaluating A260/A280 ratios using a NanoDrop 2000 spectrophotometer (Thermo Fisher Scientific). Mouse thyroid total RNA was purchased from Takara Bio (#636674). The cDNAs were synthesized using a High-Capacity cDNA Reverse Transcription Kit following standard methods (Applied Biosystems, 4368813) and stored at -20°C until further use. PCR reactions were performed in triplicates (technical replicates) using a CFX96 Real-Time System thermal cycler (Bio-Rad). For analysis, results were expressed as fold change using the gene expression levels normalized to *gapdh* mRNA levels, as indicated, using the $2^{-\Delta\Delta Ct}$ method. *Dio2* was taken as the reference gene for calculating the fold-change. The following TaqMan gene probes were purchased from Thermo Fisher Scientific: mouse *Dio1* (Mm00839358_m1), mouse *Dio2* (Mm00515664_m1), mouse *Dio3* (Mm00548953_s1), mouse *Gapdh* (Mn99999915_g1), human *DIO3* (Hs00956431_s1), human *GAPDH* (Hs02758991_g1), mouse *Pgc-1a* (Mm01208835_m1), mouse *Hr* (Mm00498963_m1) and mouse *Tshr* (Mm00442027_m1).

2.4. Immunofluorescence microscopy

Mouse or human podocytes were seeded onto glass coverslips (Marienfeld) at 20×10^3 cells/ml in 12-well plates and allowed to differentiate as described above. The cells were rinsed with ice-cold PBS and fixed with 4% PFA for 10 min at room temperature followed by permeabilization with 0.1% Triton X-100 for 5 min. After washing with PBS twice for 5 min each, the coverslips were incubated with blocking buffer in 5% donkey serum (Sigma-Aldrich, D9663) for 1 h at room temperature. For immunofluorescence staining, cells were incubated with custom rabbit anti-human D3 (1:100; Novus Biologicals, NBP1-05767; RRID:AB_1556282), and/or Mouse anti-human Synaptopodin (1:300; D-9; Santa Cruz Biotechnology, sc-515842), at 4°C overnight. The cells were washed with cold PBS and incubated with appropriate Alexa Fluor 488–labeled donkey anti-Rabbit IgG (1:1000; Molecular Probes, A-21206; RRID:AB_2535792) and/or Alexa Fluor 647–labeled donkey anti-mouse IgG (1:1000; Molecular Probes, A-31571; RRID:AB_162542) secondary antibodies at room temperature for 1 h. Cells were stained with 0.1 μg/ml DAPI (Invitrogen, D1306) in PBS. Then cells were examined using an LSM 700 laser scanning fluorescence confocal microscope with ZEN software (Zeiss).

2.5. Flow cytometry

After 12 days of differentiation, mouse podocytes were trypsinized and rinsed with PBS. In a final volume of 50 μl containing 2×10^5 cells, staining was performed with 1:50 dilution of either Rabbit anti-TSH-R-FITC conjugated antibody (Bioss Antibodies, BS-0460R-FITC; RRID:AB_11042712) or normal mouse IgG-FITC (Santa Cruz, sc-2856; RRID:AB_737238) for 1 h at 4°C. Cells were washed with FACS buffer (PBS with 0.5% BSA and 0.1% azide) twice at 1000 × g at 4°C. After the final wash, podocytes were resuspended in 50 μl PBS and were fixed with 200 μl of 1.2% paraformaldehyde in PBS. The samples were read on a FACScalibur (Beckton and Dickinson). 5000 events were collected in each case and data was analyzed using the FlowJO software.

2.6. Generation of podocyte-specific D3 knockout (D3KO) mouse model

Using a well-established Cre-loxP technology, we inactivated D3 selectively in the adult glomerular podocytes. Homozygous mice ($Dio3^{fl/fl}$), designated as D3-flox, were generated in the laboratory of Domenico Salvatore (Department of Public Health, University of Naples "Federico II," Naples, Italy) [20] and were generously donated by Antonio Bianco (Department of Medicine, University of Chicago). D3 contains a selenocysteine residue in its catalytic domain, which is encoded by an in-frame UGA stop codon. However, to override the stop codon and to insert a selenocysteine instead, a cis-acting stem loop sequence called as the selenocysteine insertion sequence (SECIS) is required in the 3′ UTR of the mRNA [21]. Since SECIS element is essential for the full-length translation of D3 protein, this region was ablated in the *Dio3* gene. To accomplish that, a plasmid harboring floxed sites in the *Dio3* locus, and specifically flanking the SECIS mRNA structure located at nt 1,001 and nt 1,706 from the ATG in the *Dio3* mRNA was generated. In the absence of the SECIS, the TGA codon within the D3 catalytic domain will be recognized as stop codon, and the protein translation will be terminated [20]. We crossed these D3-flox mice with the driver mouse strain expressing Cre recombinase under podocyte-specific *Nphs2* promoter (Pod-Cre mice) (obtained from Jackson Laboratory) to generate D3KO mice ($Pod\text{-}Cre^{+/-}$::$Dio3^{flox/flox}$). All mice were crossed onto a pure C57BL/6J (B6) background. In the presence of the Pod-Cre transgene, D3KO mice will have podocyte-specific excision of the floxed Dio3 SECIS, resulting in a null allele with termination at the UGA codon and no D3 catalytic activity. Podocin-Cre littermates served as controls. The expected recombination event occurred in the progeny, which was confirmed by tail clip genotyping using CflipU and FflipL primers to confirm lox sites and pod-cre-f and pod-cre-r primers to confirm cre sites. Further to validate lack of D3 expression in the podocytes of D3KO mice, primary podocytes were isolated from glomeruli of 10-week old D3KO mice or littermates controls as described below in section 2.7. Western blot analysis was done using rabbit anti-D3 antibody (10 μg/ml, Novus Biologicals # NBP1-05767) and relative density of D3 bands was calculated via ImageJ software, normalized to the GAPDH, and compared to littermate controls (n=3 per group).

2.7. Isolation of primary podocytes

Primary mouse podocytes were isolated using Dynabeads magnetic separation as described previously [22] with some modifications. Briefly, mice (Male, Wild-type (C57BL/6) or Lox-D3 (no podocin-cre), 8-10 weeks old) were anesthetized and perfused through the heart with 20 ml Hank's Balanced Salt Solution (HBSS), which contained 8×10^7 M-450 Dynabeads (Invitrogen, 14013). Kidneys were harvested, minced into small pieces, and digested at 37°C for 30 min in HBSS buffer containing 1 mg/ml collagenase A (Sigma-Aldrich, C-6885) and 100 U/ml DNase I (New England Biolabs, M0303L). The digested tissue was then passed twice through a 100 μm nylon mesh (BD Biosciences, 352360), washed with HBSS buffer followed by isolation of magnetic particles. Isolated glomeruli were then cultured for 5 days on dishes previously coated with collagen I. Cells were trypsinized, filtered using a 40-μm cell strainer (BD Biosciences, 352340), centrifuged and seeded on collagen I–coated dishes for sub-culturing.

2.8. LPS-induced proteinuric and hypothyroid mouse models

Proteinuria was induced in mice as described previously [23] with some modifications. Mice were intraperitoneally injected with a single dose of LPS-EB at 2.5 mg/kg body weight followed by a single intraperitoneal injection of 150 μl of iopanoic acid (IOP) in 2% (v/v) ethanol solution (0.11 g/kg) [24]. Ethanol alone was used as a vehicle control. After 24 h, the kidneys were removed and processed for microscopy as described is subsequent sections.

2.9. Measurement of ACR levels

Mouse urine samples were collected for the measurement of urinary albumin and creatinine using a mouse albumin ELISA kit (Bethyl Laboratories, E99-134), and a creatinine assay kit (Cayman Chemical, 500701), respectively, according to the instructions provided in the kit. The ratio of urinary albumin to creatinine (ACR, mg/g) was then calculated.

2.10. Electron microscopy (EM)

Kidneys were extracted from the control and treated mice. Renal tissue was first fixed in PFA overnight at 4°C and post-fixed for 1 h in 1% osmium tetroxide (OsO4) on ice. Tissues were washed, dehydrated, and embedded in Embed 812 Resin (Electron Microscopy Sciences, 14120). Ultrathin kidney sections (70 nm) obtained on the EM UC7 Ultramicrotome (Leica) were placed on Formvar-coated nickel grids (EMS, FF-2010-Ni) and counter stained with 5% uranyl acetate and 0.1% lead citrate. EM micrographs were taken using a Sigma HD VP Electron Microscope (Zeiss). Foot process effacement was quantified from transmission electron microscopy (TEM) micrographs of glomeruli as described previously [25]. Briefly, multiple capillary loops were imaged at 5000 × and glomerular basement membrane (GBM) length was measured for 10 different glomeruli from a minimum of 4 mice per condition using ImageJ software (version 1.52a; National Institutes of Health). To quantify effacement, secondary processes (i.e., foot processes, FPs) were tallied manually, and this was divided by the length of GBM examined to calculate FPs per unit length (i.e., μm of GBM).

2.11. Western blotting

Total cell lysates (10 μg) in RIPA buffer were supplemented with Halt protease and phosphatase inhibitor cocktails (Thermo Fisher Scientific). For fractionated samples, lysates corresponding to at least 25-50 μg were used. Plasma Membrane Protein Extraction Kit for organelle fractionation and NE-PER^{TM} Nuclear and Cytoplasmic Extraction Reagents were used for cellular fractionation (Abcam, ab65400) according to the manufacturer's protocol. The samples were separated on SDS-PAGE gradient gel (NuPAGE 4−12% Bis-Tris, Invitrogen) followed by transfer to nitrocellulose membrane (LI-COR Biosciences, 926-31092). Blots were blocked using TBS-based Odyssey blocking buffer (LI-COR Biosciences, 927-50000) or 5% blotting grade skimmed milk (Bio-Rad) in TBST for 1 h at room temperature with constant shaking. Blots were incubated with primary antibodies [Cell signaling technology: total Src #2108 (RRID:AB_331137), phospho-Src (Y416) D49G4 #6943S (RRID:AB_10013641), total PKCα #2056T (RRID:AB_2284227), phospho-PKCα/β II (Thr638/641) #9375T (RRID:AB_2284224), total FAK #3285T (RRID:AB_2269034), phospho-FAK (Tyr397) #3283S (RRID:AB_2173659), phospho-Paxillin (Tyr118) #2541S (RRID:AB_2174466), total Paxillin (D9G12) #12065S (RRID:AB_2797814), total ERK1/2-HRP conjugated #4348 (RRID:AB_10693601), phospho-ERK1/2 (T202/Y204) #9101S (RRID: AB_331646); Abcam: phospho-Paxillin (Tyr 113) #ab32084 (RRID: AB_779033); Santa Cruz: p-PKCα (A11) #Sc-377565 (RRID: AB_2877652)] diluted in TBS-Tween (either with skimmed milk or BSA as recommended by the supplier) overnight at 4°C with gentle rotation. IRDye 800RD donkey anti-rabbit IgG (H+L) (LI-COR Biosciences, 926-32213; RRID AB_621848) and IRDye 800 donkey anti-mouse IgG (H+L) (LI-COR Biosciences, 926-32212; RRID AB_621847) were used as secondary antibodies, diluted in TBST for 1 h at room temperature. The protein detection and image capture were performed using an Odyssey CLx imaging system (LI-COR Biosciences).

2.12. Ultra-performance liquid chromatography (UPLC)

In brief, 10-day-old differentiated mouse podocytes were placed in serum-free medium for 24 h prior to T3 (10^{-7} M) treatment. Cells are then washed in PBS, harvested in buffer (PBS containing 2 mM EDTA, 1 mM DTT and protease inhibitor cocktail), pelleted and either analyzed right away or snap frozen and stored at -80 until analysis. Cell pellets were processed in UPKC lysate buffer (PBS containing 1 mM EDTA, 10 mM DTT with 0.25 M sucrose) and lysates are used for D3 activity assay as described [26].

2.13. Molecular cloning and purification of recombinant human D3 protein

The gene encoding full length human *DIO3* was codon optimized and synthesized as linear DNA strand (G-block, Integrated DNA Technologies) for subsequent cloning procedures. This fragment was cloned in-frame with N-terminal GFP and 6x-His tag after digestion with the restriction enzyme *Ssp*I using Gibson cloning into a commercially available plasmid from Adgene (pET His6 GFP TEV LIC cloning vector [1GFP], plasmid 29663). Expression of GFP-tagged full-length D3 (1-304 aa), abbreviated as $D3^{FL}$ was induced in BL21(λDE3) cells at 25°C for 16 h in enriched terrific broth. Cell pellets were subjected to three cycles of repeated freeze-thaw followed by lysis using sonication in sonication buffer (25 mM HEPES, pH 8.0, 500 mM NaCl, 2.5 mM imidazole, 5% sucrose wt/vol, 0.1% Triton X-100) then spun at 35,000 rpm for 45 min. The soluble fraction was incubated with 4 ml of 50% Nickel immobilized metal ion affinity chromatography resin (Qiagen) for 2 h at 4°C. The beads were washed extensively with 100 ml wash buffer (25 mM HEPES, pH 8.0, 500 mM NaCl, 2.5 mM imidazole, 5% sucrose wt/vol) and eluted with a gradient of 50-500 mM imidazole. Fractions containing the proteins were pooled and subjected to dialysis in PBS. The protein was determined to be ~>95% pure using SDS-PAGE analysis. Protein concentration was estimated using both a spectrophotometer and a BCA protein estimation kit. Protein was flash frozen in liquid nitrogen and stored at −80°C until further use.

2.14. Surface plasmon resonance (SPR)

Protein interactions were measured and analyzed on a Biacore T200 instrument (GE Healthcare). Experiments were performed at 25°C. Briefly, to measure the binding affinities of the candidate analyte proteins [human- integrin $\alpha v\beta 3$ (R&D Systems, 3050-AV-050) and human uPAR (R&D Systems, 807-UK-100/CF)] to recombinant human $D3^{FL}$ protein, the latter protein was immobilized on to the flow channel on a CM5 sensor chip using a standard amine coupling method. For immobilization, $D3^{FL}$ was diluted in 10 mM sodium acetate, pH 4.5, and was loaded on to the chip after activation of the sensor surface with catalyst (3-dimethylaminopropyl)-3-ethylcarbodiimide (EDC)-N-hydroxysuccinimide (NHS), followed by blocking of the unoccupied surface area using 1M ethanolamine. Integrin $\alpha v\beta 3$ protein, in a series of increasing concentrations (i.e., 0-150 nM in 2-fold serial dilutions), was applied to the channels as an analyte at a flow rate of 25 μl/min. The running buffer for the binding experiments was 10 mM HEPES, 150 mM NaCl, 0.05% n-Octyl-β-D-glucopyranoside, pH 7.1. To study the binding of analytes to activated integrin, 2 mM $MnCl_2$ and 0.1 mM $MgCl_2$ were added to the binding

buffer. For inhibition, a combination of cRGDfv and Tetrac (15 μM each) was pre-incubated with increasing concentrations of $\alpha v\beta 3$ integrin during sample preparation on a plate and injected following the same procedure as previously described. Data were double-referenced with blank (ethanolamine) RU values on flow channel 1 and zero concentration analyte signal. Sensorgrams were analyzed using the Biacore T200 evaluation software 2.0.3, and response units (RU) were measured during the equilibration phase at each concentration for steady-state affinity fittings. Kinetic fittings were done by 1 to 1 Langmuir binding model embedded within the Biacore T200 evaluation software 2.0.3.

2.15. Co-immunoprecipitation

Cultured HEK293T cells (procured from ATCC; RRID:CVCL_0063) were grown at 37°C with 5% CO_2 in Dulbecco's Modified Eagle's medium (DMEM, Life Technologies) containing 10% fetal bovine serum, 100 U/ml penicillin and 1 μg/ml streptomycin, until 50-60% confluence was reached. Transfection of plasmids was carried out using FuGENE® HD Transfection Reagent (Promega) for 48 h according to the manufacturer's protocol. The plasmid used for transfection of *DIO3*, NM_001362 (abbreviated as D3Cys) from GenScript (OHu24700D), contained a C-terminal FLAG tag and a stop codon TGA which is read as Selenocysteine. This stop codon was replaced with codon for Cysteine (Cys) using site-directed mutagenesis for efficient translation in the HEK-293T cells. The plasmid used for transfection of Integrin $\beta 3$ (NM_000212.2) was procured from Sino Biologicals (HG10787-CM) contained a C-terminal Myc tag. The transfected cells were harvested; washed with 1 × PBS twice and were lysed in RIPA buffer supplemented with protease inhibitor (Roche). One percent of the cell lysate volume was loaded as the input to assess the presence of desired proteins in each case. One mg total cell protein was used per IP and isotype control mouse IgG antibody were used along with antibodies against: FLAG (F1804, Sigma; RRID:AB_262044) and c-Myc (Origene, clone OTI3F2, formerly 3F2, TA500003, RRID:AB_2148581). Anti-FLAG M2 affinity (Sigma), anti-c-Myc agarose and protein A/G beads (Pierce, Thermo Fisher Scientific) were used to isolate protein-antibody complexes, then eluted by boiling the beads with 2 × Laemmli reducing sample buffer (Invitrogen). Proteins were resolved on 4–12% Bis-Tris NuPAGE (Invitrogen) gels and transferred to the nitrocellulose membrane (LI-COR Biosciences) for Western blotting. The interacting partners were detected by Western blotting using the appropriate antibodies and developed as described above using an Odyssey CLx imaging system (LI-COR Biosciences).

2.16. In vitro scratch assay

An artificial gap, or 'scratch' was created on a confluent monolayer of differentiated mouse podocytes using a 200 μl plastic pipette tip. The detached cells were removed by washing the wells twice with 1 × PBS followed by the addition of fresh growth medium in the presence or absence of T3 (10^{-7} M) or PAN (30 μg/ml). Brightfield microscopy images were taken immediately after the creation of the scratch and were considered as T_0. After 24 and 48 h post treatment, images were captured again at T_{24} and T_{48}. The area covered or migrated in each case was quantified and calculated using Image J software. The images were saved as 8-bit multi-page TIFF files before data analysis. Experiments were performed in triplicate.

2.17. In situ Proximity ligation assay (PLA)

PLA was performed using Duolink® in Situ Orange Starter Kit for Mouse/Rabbit antibody combination (Sigma Aldrich, DUO92102) according to the manufacturer's instructions. This kit included mouse and rabbit secondary antibodies with probes, blocking solution, wash buffers A and B, amplification solution, ligase solution and detection reagent. Human biopsy kidney sections were rinsed with ice-cold PBS and fixed with 4% PFA for 10 min at room temperature followed by permeabilization with 0.1% Triton X-100 for 5 min. After washing with PBS twice for 5 min each, the tissues were blocked for 1 h with agitation in the PLA blocking solution (Duolink®). After the blocking step, slides were incubated with a combination of either (a) rabbit anti-D3 (10 μg/ml, Novus Biologicals # NBP1-05767) and mouse anti-$\alpha v\beta 3$ (10 μg/ml, Abcam clone LM609 # ab190147) antibodies, or (b) 10 μg/ml each of normal rabbit IgG (Santa Cruz Biotechnology, sc-2027; RRID:AB_737197) and normal mouse IgG (Santa Cruz Biotechnology, sc-2025; RRID:AB_737182) as controls, diluted in Duolink® antibody dilution buffer, overnight at 4°C. This was followed by incubation with secondary antibodies conjugated with complementary oligonucleotide PLA probe PLUS (anti-rabbit PLUS: DUO92002; RRID:AB_2810940) and MINUS (anti-mouse MINUS: DUO92004; RRID:AB_2713942) at 37°C for 1 h. The ligation (30 min), amplification (100 min) and washing steps with Buffers A and B were performed exactly as recommended. All incubations were performed in humidified chamber. The slides were stained with DAPI and mounted using Confocal images were captured using an LSM 700 laser scanning fluorescence confocal microscope equipped with ZEN software (Zeiss). Mean fluorescence intensity (MFI) was measured using ImageJ software (version 1.52a; NIH). Each disease group was normalized to healthy controls and is shown as fold change.

2.18. Measurement of cAMP levels

Twelve days old differentiated and serum starved mouse podocytes (1×10^6 in 6-well plate) were exposed to 50 nM TSH, normal rabbit IgG isotype or anti-TSH-R antibody (3 μg/ml each) or a known adenylate cyclase activator, Forskolin (50 μM) (Tocris Bioscience #1099) for 1 h. cAMP (pmol/ml) was measured in the culture supernatants using Mouse/Rat cAMP Parameter Assay Kit from R&D Systems (#KGE012B), based on competitive enzyme immunoassay, exactly according to the manufacturer's instructions. Briefly, to 200 μL culture supernatants, 40 μL of 1N HCl was added to inactivate the phosphodiesterases. The samples were incubated for 10 min at room temperature followed by neutralization with 40 μL of 1N NaOH. Samples were then diluted with 280 μL of Calibrator Diluent RD5-55 and assayed immediately.

2.19. Statistics

Statistical analysis was calculated using Prism 6.0 software (GraphPad). Data are presented as mean ± SEM. For comparison of two groups, statistical significance was evaluated using an unpaired two–tailed Student's *t*–tests with an assumption that the data were normally distributed. All *P* values less than or equal to 0.05 were considered significant and are indicated in the text as appropriate, $^{*}P < 0.05$, $^{**}P < 0.01$, $^{***}P < 0.001$, and $^{****}P < 0.0001$.

2.20. Human and animal subjects study approval

All animal experiments were carried out according to the NIH's Guide for the Care and Use of Experimental Animals (National Academies Press, 2011), and approved by the Institutional Animal Care and Use Committee (IACUC#18-049) at Rush University (Chicago, Illinois, USA). Human biopsy kidney sections from healthy donors and patients with FSGS, DN and MCD were procured after informed consent and in accordance with the guidelines on human research and with approval of the Institutional Review Board (#14051401-IRB01) of Rush University Medical Center (Chicago, Illinois, USA).

Role of funding source

This work was supported by American Thyroid Association (ATA-2018-050.R1). However, the funding agency has no role in conceptualization or design of this study; neither in the collection, analysis, and interpretation of the data; nor in the writing or the decision to submit the paper for publication.

3. Results

3.1. Injured podocytes display reduced Dio3 expression

To understand how TH effects are regulated in podocytes, we first sought to establish the relative expression levels of the 3 different deiodinases that function to either activate (D1 or D2) or inactivate (D3) TH (Fig. 1a). The qPCR data revealed that the *Dio3* transcript was the most abundant in cultured mouse podocytes (>20-fold compared to *DIO2*) whereas only minimal expression of *Dio1* could be found (Fig. 1b). We next sought to assess *Dio3* mRNA profile after podocytes were exposed to stress-inducing conditions. Cultured mouse and human podocytes were treated with puromycin aminoglycoside (PAN) (Fig. 1c) or LPS (Fig. 1d), respectively, both of which reduced *Dio3* mRNA levels. These findings were in accordance with publicly available database in the Nephroseq (The Regents of the University of Michigan, Ann Arbor, MI), which shows that *DIO3* mRNA levels were reduced in the glomeruli and tubulointestitial compartments of patients with chronic kidney disease such as FSGS, in addition to those who had acute kidney rejection after transplantation (Fig. 1e).

3.2. The subcellular localization of D3 and its activity are altered upon injury to podocytes

To evaluate the consequence of stress-inducing conditions on the cell membrane D3 expression, mouse podocytes were injured using

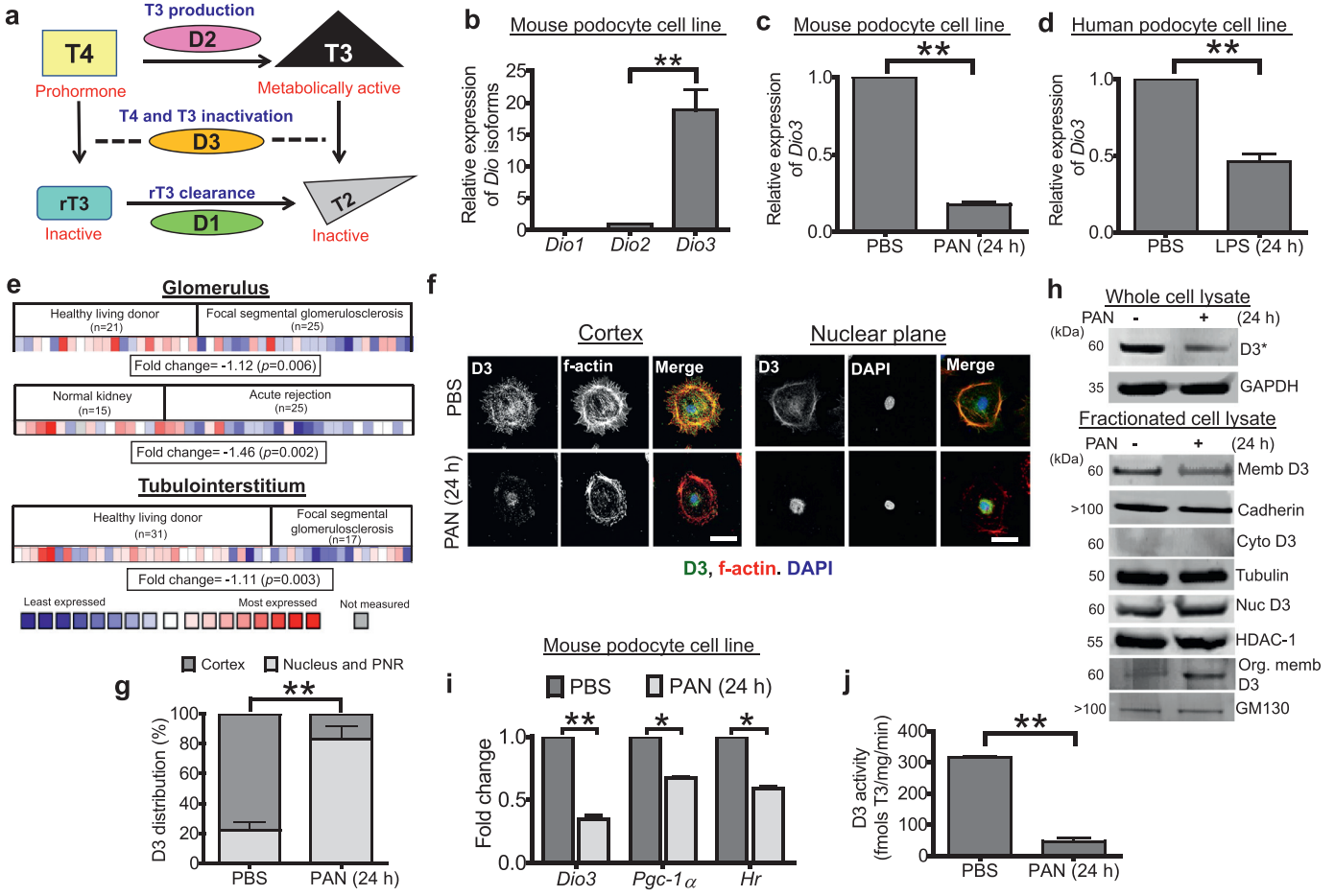

Fig. 1. Deiodinase 3 (*DIO3*, D3) is the abundant isoform in mouse podocytes. (a) Schematic showing Deiodinase type II (D2) converts the initially released hormone precursor thyroxine (T4) to T3. D3 inactivates T3, the active form of TH, via reductive elimination of iodine. (b) qPCR analysis of deiodinases in mouse podocytes in comparison to the housekeeping gene *gapdh*, with *DIO2* as the reference; $^{**}p \leq 0.01$ determined using non-parametric Students *t*-test. (c) qPCR analysis of *DIO3* in mouse podocytes upon PAN (30 μg/ml for 24 h). *gapdh*, was used as the housekeeping gene with *DIO2* as the reference; $^{**}p \leq 0.01$ determined using non-parametric Students *t*-test. (d) qPCR analysis of *DIO3* in human podocytes upon LPS (50 μg/ml for 24 h) addition. *gapdh*, was used as the housekeeping gene with *DIO2* as the reference; $^{**}p \leq 0.01$ determined using non-parametric Students *t*-test. (e) The Nephroseq database indicating expression profiles for *DIO3* transcript in different renal cell types under the indicated conditions. The fold-change (log2 median-centered intensity) and the *p* values are also indicated in a box below each array. Key depicting the range of expression from least expressed (blue) to the most (red) and not measured (light gray) is shown below. (f) Confocal micrograph capturing the cortex of untreated (UT) or PAN treated mouse podocytes 24 h post treatment in the top panel. Bottom panels show the nuclear plane of the same samples. D3 and actin co-localization at the cortex of the podocyte is seen. Stains: Left column, grayscale of α-D3; middle column, grayscale of F-actin; right column, merge of α-D3 in green, f-actin in red, DAPI in blue. Scale bar=50 μm. (g) Quantification of D3 fluorescence intensity distribution as observed in podocytes in f, $^{**}p \leq 0.01$. (h) Western blot analysis of D3 in different cellular compartments obtained by fractionating mouse podocytes. Purity of the fractions was determined by using Cadherin, membrane marker; Tubulin, cytoplasmic marker; HDAC-1, nuclear marker and GM 130, Golgi marker. *D3 is known to migrate as a dimer at ~60 kDa. (i) qPCR analysis of *HR* and *PGC-1α* in mouse podocytes upon PAN (30 μg/ml for 24 h) treatment. *gapdh*, was used as the housekeeping gene; $^{**}p \leq 0.01$ *and* $^{*}p \leq 0.05$ determined using non-parametric Students *t*-test. (j) D3 enzymatic activity was measured using UPLC. The peaks correlating with deiodination products of TH in total lysates from untreated *vs.* PAN treated (24 h) mouse podocytes were quantified and T3 to T2 conversion rate is plotted, $^{**}p \leq 0.01$.

PAN and analyzed for D3 subcellular localization. Notably, 24 h-post PAN treatment, confocal micrographs show a dramatic reduction of D3 expression at the plasma membrane of injured podocytes (Fig. 1f, left panel). An optical section through the nuclear plane further revealed that D3 expression was compartmentalized and enhanced in the nucleus and perinuclear regions (PNR) (Fig. 1f, right panel). Moreover, the co-localization of D3 with cortical F-actin, which was evident in the untreated podocytes, was lost upon PAN treatment (Fig. 1f, right panel). Quantification of the fluorescence intensities revealed that the subcellular localization of D3 switched from plasma membrane to nuclear after PAN treatment. In PBS-treated control cells, 22±5% of the D3 signal was found in the nucleus. This percentage increased to 82±8% in podocytes treated with PAN (Fig. 1g). Western blots performed on the fractionated cellular compartments also showed enhanced D3 levels in the nuclear and organelle compartments after PAN treatment with a concomitant loss of total D3 and a reduction in the plasma membrane fraction (Fig. 1h). To confirm that this subcellular redistribution also occurs in cultured human podocytes, D3 localization was assessed after LPS treatment. Confocal images show that LPS-treated human podocytes also displayed a loss in the plasma membrane D3 and an increased concentration of D3 signal in the nucleus and Golgi, as indicated by co-localization with the Golgi marker GM-130 (Supplementary Fig. 1).

To assess if nuclear accumulation of D3 in PAN-injured podocytes corroborates with a reduced transcription of T3-responsive genes, we performed qPCR to detect the mRNA levels of *peroxisome proliferator-activated receptor-γ coactivator-1α (Pgc-1α)* and *Hairless (Hr)*. As anticipated, transcript levels of *Pgc-1α* and *Hr* were decreased in PAN-treated mouse podocytes compared to the untreated cells (Fig. 1i); indicating that nuclear D3 could degrade the residual T3 in the nucleus, which dampened the transcription of genes positively regulated by T3.

Next, we studied D3 activity (i.e., conversion of T3 to T2) in the cell lysates of PAN-treated mouse podocytes by adding ^{125}I-T3 and measuring deiodination products via ultra-performance liquid chromatography (UPLC). Indeed, D3 activity in PAN-injured podocytes dropped markedly (Fig. 1j).

3.3. TH signaling modulates cytoskeletal organization and D3 subcellular distribution

Next, we wished to bypass D3 and increase T3 signaling in podocytes by exposing mouse podocytes to 100 nM T3 while the cells were kept in 2% charcoal stripped FBS. Similar to PAN-treatment, exposure of T3 for 48 h was sufficient to cause phenotypic changes in podocytes as evident in the confocal micrographs of phalloidin-stained cells. There was a loss of F-actin polarity (Fig. 2a) and an increase in cell size (Fig. 2b). Also, T3 reduced plasma membrane D3 while increasing it in the cell nucleus (Fig. 2a). Our data suggest that increasing TH signaling in podocytes elicits a cellular response that resembles PAN treatment, i.e., redirection of D3 to the cell nucleus and loss of cytoskeletal organization.

3.4. T3 activates integrin signaling in podocytes

Recently, $\alpha v\beta 3$ integrin has been identified as a receptor for T3 [27]. Therefore, we treated mouse podocytes with T3 to test whether TH action produces downstream signaling via $\alpha v\beta 3$ integrin receptor. Indeed, incubation with T3 caused an increase (1.5-2-fold) in the phosphorylation of FAK at Tyr397, PKC-α at Ser634 and Thr638/641, paxillin at Tyr118 and Tyr113, and Src kinase at Tyr416 (Fig. 2c, d). There are two T3-binding sites on $\alpha v\beta 3$ integrin, Site-1 and Site-2. Although, both sites are sensitive to inhibition by Tetrac, Site-1 can be blocked only by the cRGDfv peptide, an $\alpha v\beta 3$ integrin inhibitor [28]. Therefore, initially we were unable to block T3-mediated activation of $\alpha v\beta 3$ integrin signaling using only cRGDfv; however, addition of cRGDfv and Tetrac together for 2 h prior to T3 exposure diminished the activation of the $\alpha v\beta 3$ integrin-mediated downstream signaling factors (Fig. 2e).

An early event following integrin activation on podocytes is increased motility [4]. We therefore measured the podocyte migration rate upon T3 treatment. For this, a scratch assay was employed where mouse podocytes in the monolayer were vertically scratched using a pipette tip and then treated with either T3 or PAN, a known promoter of podocyte motility [29]. Both T3 and PAN treated podocytes migrated twice as fast than the untreated controls (Fig. 2f, g).

Previous studies have shown that T3 induced phosphorylation of ERK1/2 via $\alpha v\beta 3$ integrin, followed by cellular proliferation and migration in several cancer cell lines [30]. We sought to determine if a similar mechanism was acting in T3-treated podocytes. We observed phosphorylation of ERK1/2 in mouse podocytes upon T3 treatment in as early as 20 min (Fig. 2h, i), which was inhibited by adding a combination of both cRGDfv and Tetrac. This suggests that the $\alpha v\beta 3$ integrin receptor expressed on podocytes may play a pivotal role in responding to and integrating T3 signaling, effectively acting as a focal point for crosstalk between the thyroid-kidney axis.

3.5. D3 interacts with the $\alpha v\beta 3$ integrin receptor

The presence of D3 in the plasma membrane raises the possibility that it could interact with $\alpha v\beta 3$ integrin. To test this hypothesis, FLAG-tagged CysD3 and Myc-tagged $\beta 3$ integrin were transiently co-expressed in HEK-293T cells. Indeed, immunoprecipitation using anti-FLAG antibody pulled down both D3 and $\beta 3$ integrin (Fig. 3a, left panel). In a reciprocal experiment, the pull down of Myc-tagged-$\beta 3$ integrin with anti-Myc antibody was able to immunoprecipitate FLAG-tagged D3 (Fig. 3b). This interaction seems to be highly specific, given that we were not able to pull down FLAG-tagged CysD3 using anti-Myc antibody from cells co-transfected with FLAG/Myc-tagged $\beta 1$ integrin and CysD3 (Fig. 3a, right panel).

To further test the direct binding of D3 with $\alpha v\beta 3$ integrin and to measure the strength of this interaction, we used Surface Plasmon Resonance (SPR). Full-length recombinant D3 ($D3^{FL}$) was bacterially expressed, purified, and used for the analysis (Fig. 3c). The sensorgrams revealed that $D3^{FL}$ could directly bind $\alpha v\beta 3$ integrin with a K_D of 16 nM (Fig. 3d). Addition of Mn^{2+}, a potent integrin activator, did not substantially alter the binding affinity (K_D of 45 nM) between the two proteins (Fig. 3e). We also tested if the binding between D3 and $\alpha v\beta 3$ integrin could be competitively inhibited by cRGDfv and/or Tetrac. Remarkably, pre-incubation of $\alpha v\beta 3$ with cRGDfv alone resulted in marked reduction in binding affinity of the receptor to $D3^{FL}$, K_D=2107 nM (Fig. 3f). However, a combination of cRGDfv with Tetrac almost abolished binding with $D3^{FL}$, K_D>2mM (Fig. 3g), indicating that the interaction between $D3^{FL}$ and $\alpha v\beta 3$ integrin is quite specific. Neither the cRGDfv inhibitor alone nor in combination with Tetrac were able to bind to the immobilized $D3^{FL}$ (Supplementary Fig. 2).

It is noteworthy that SPR data are in consonance with our Western blot data in Figure 2, wherein complete inhibition of integrin signaling via T3 is observed only when both inhibitors are used. In agreement with the SPR data, co-immunoprecipitation of Myc-tagged $\beta 3$-integrin by FLAG-tagged D3 was also compromised at least 2-fold when the plasmids were transfected in the presence of both the inhibitors (Fig. 3h). Taken together, our data strongly suggest that D3 interacts with $\alpha v\beta 3$ integrin.

To demonstrate a viable *in situ* interaction between D3 and $\alpha v\beta 3$ integrin in healthy podocytes and its loss in diseased conditions, a Proximity Ligation Assay (PLA) was used on human kidney biopsies from healthy individuals and from patients with FSGS, DN or MCD. While the tissue from healthy donors showed the appearance of orange punctate-like fluorescence indicating a positive interaction between D3 and $\alpha v\beta 3$ integrin, the tissues obtained from diseased samples showed a significant reduction in the fluorescence

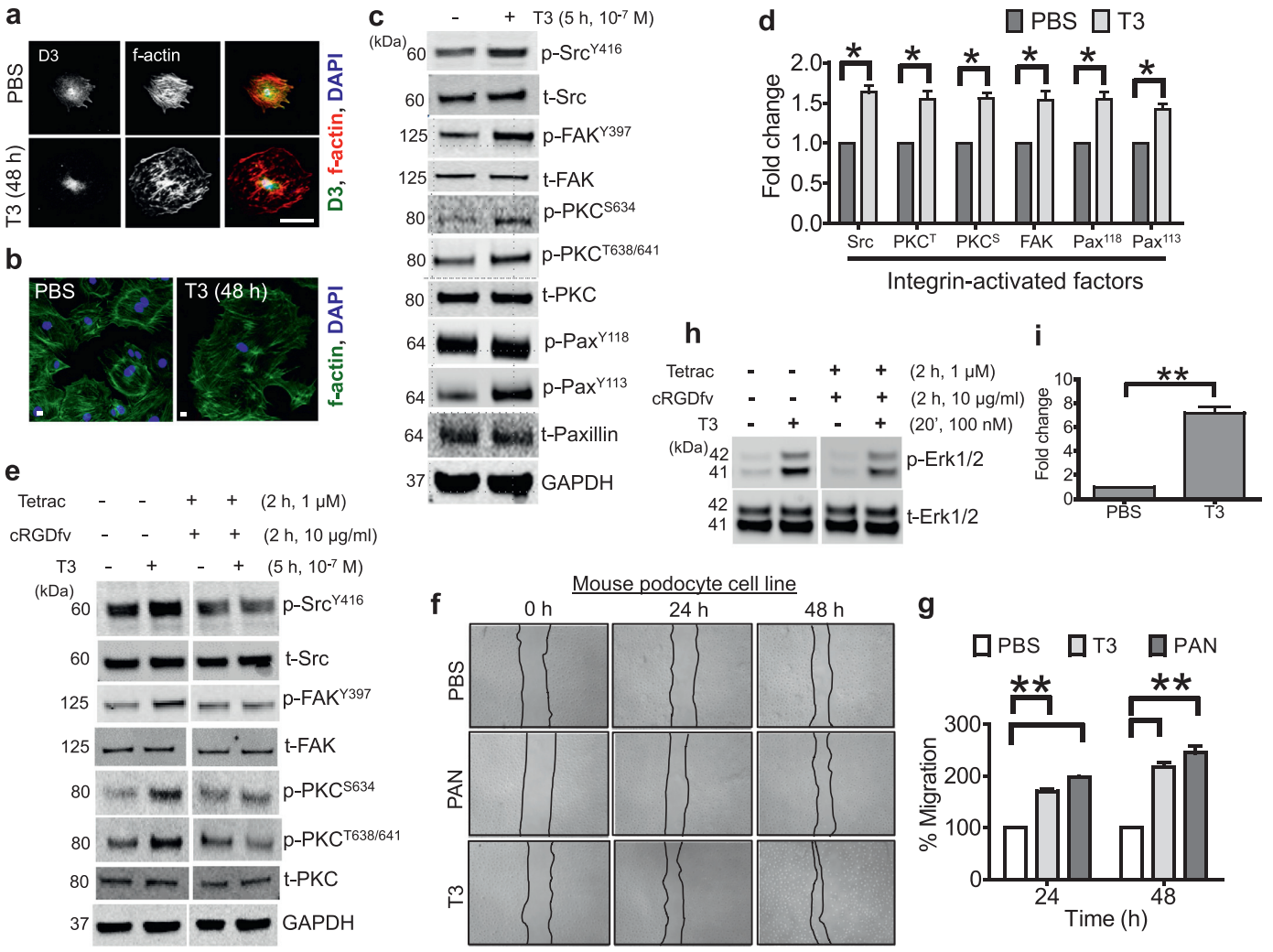

Fig. 2. Excess TH signaling (hyperthyroidism) affects cytoskeletal organization, induces $\alpha v\beta 3$ integrin signaling and increased migration and injury in mouse podocytes. (a) Confocal micrographs of cultured mouse podocytes left untreated (UT) or T3 treated (10^{-7} M) for 48 h. Stains: Left column, grayscale of α-D3; middle column, grayscale of F-actin; right column, merge of α-D3 in green, F-actin in red, DAPI in blue. Scale bar=50 μm. (b) Shown is the merged confocal micrograph of cultured mouse podocytes untreated (UT) or T3 treated (10^{-7} M) stained for F-actin with Phalloidin-488 (green) and DAPI (blue). Scale bar=10 μm. (c) Western blot analysis of podocytes treated with 10^{-7} M T3 for 5 h and probed with the indicated antibodies. Representative blot from three independent experiments is shown. Migration of molecular weight standards is depicted on the left as kDa. (d) Quantification of the band intensities was performed for blots shown in c, using LiCOR-Biosciences odyssey software. The fold change in the expression level was calculated by normalizing the phosphorylated factors with their total counterparts and PBS treated podocytes were considered as the baseline. Also, GAPDH was used as a loading control. Non-parametric two-tailed Students *t*-test was used to calculate the significance, $^{*}p \leq 0.05$. (e) Western blot analysis of podocytes treated with 10^{-7} M T3 for 5 h either alone as control or in the presence of inhibitor cocktail (cRGD, 10 μg/ml and Tetrac, 1 μM) for 2 h before T3 treatment. The blots were probed with the indicated antibodies. Representative blot from three independent experiments is shown. Migration of molecular weight standards is depicted on the left as kDa. (f) A "wound" was generated by creating a straight-line scratch using micropipette across an 80% confluent mouse podocyte monolayer in a 12 well plate in independent triplicates. Cells were treated with 10^{-7} M T3 or 30 μg/ml PAN as positive control and images were captured at time 0, 24 and 48 h. Representative bright-field images show acceleration of wound closure upon T3 treatment as compared to the untreated. Dotted lines define the area lacking the cells. (g) Quantification of the data shown in f. The area migrated or wound closure in percentage was calculated using Image J software as: A_{0h} (Area of the wound at 0 h i.e. immediately after the scratch was performed)-A_{xh} (Area of the wound measured at a given hour after the scratch was introduced)/A_{0h}. Non-parametric two-tailed Students *t*-test was used to calculate the significance, $^{**}p \leq 0.01$. (h) Western blot analysis of podocytes treated with 10^{-7} M T3 for 20 min and probed with phospho- and total ERK1/2 antibodies. (i) Quantification of the band intensities as obtained in h, is depicted. Non-parametric two-tailed Students *t*-test was used to calculate the significance, $^{**}p \leq 0.01$.

intensities (Fig. 3i). Faint or no signal from the IgG isotype control antibodies obviated the possibility of non-specificity.

Since urokinase receptor (uPAR) has been shown to bind to and activate podocyte $\beta 3$ integrins causing outside-in activation of the FP microfilament system, podocyte FP motility, and thus their effacement [31], we wanted to test if D3 could bind to human uPAR using SPR. The rationale was if D3 can form a complex with uPAR, this bipartite unit might bind to and activate $\alpha v\beta 3$ integrin more effectively than the individual proteins, thereby augmenting integrin-mediated podocytopathies. However, no appreciable binding between D3 and uPAR was observed ($K_D \geq 2$ mM; data not shown).

3.6. D3 expression is reduced in the glomeruli of LPS injected mice

To determine if the phenotypes observed in injured cultured mouse podocytes can be recapitulated *in vivo*, we induced acute kidney injury in mice by LPS injection. Mice were challenged with LPS for 24 h and their glomeruli were isolated and stained for D3 and synaptopodin. Consistent with our *in vitro* data, confocal analysis clearly showed a reduction of D3 staining in the glomeruli of LPS-treated mice (Fig. 4a). Quantification of the fluorescent signals revealed that D3 levels in LPS-treated mice declined by at least 2-fold compared to the untreated controls (Fig. 4b). The qPCR analysis further corroborated the confocal data and showed a significant decline in the *Dio3*

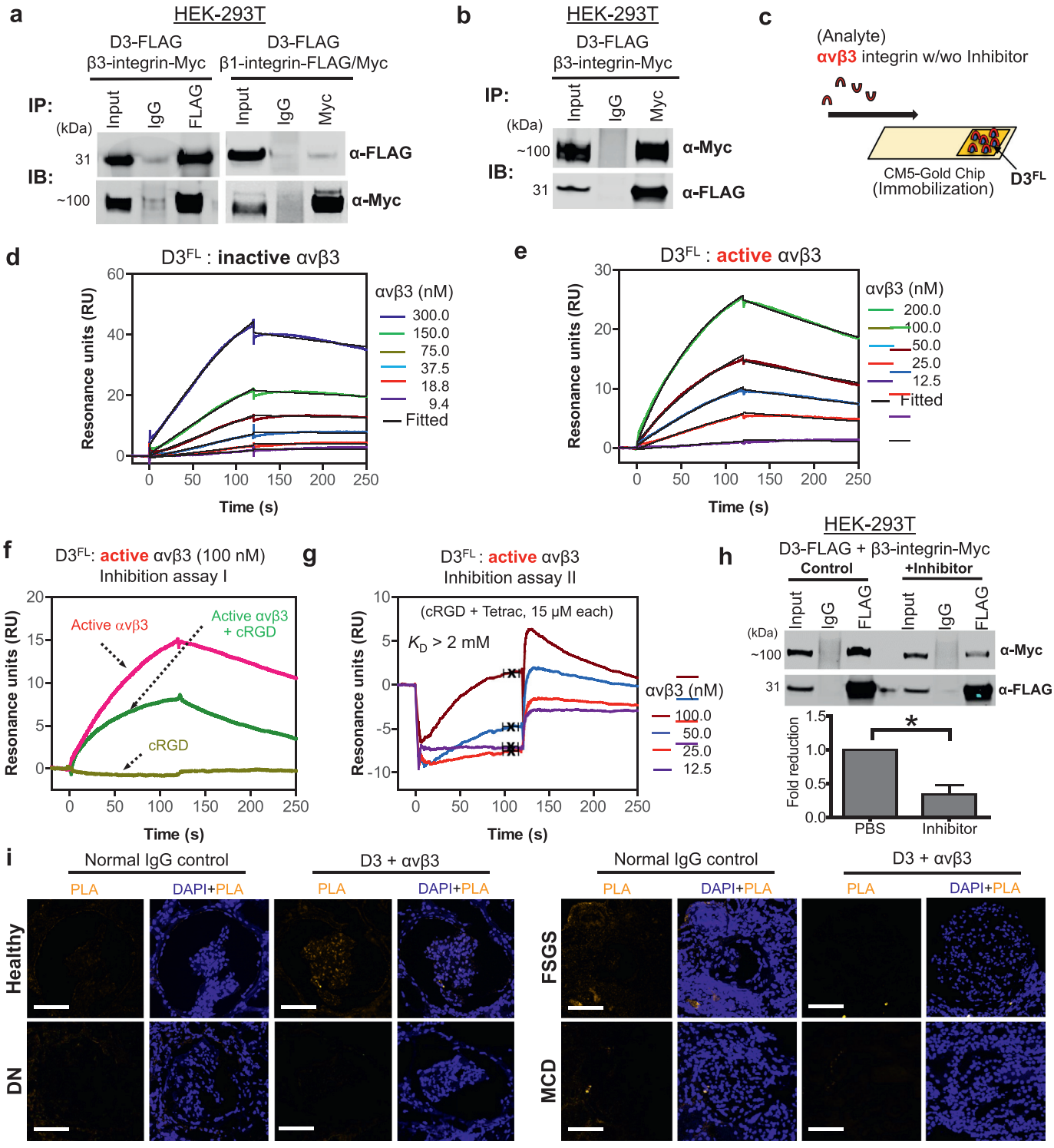

Fig. 3. D3 directly binds to $\alpha v\beta 3$ integrin. (a) HEK-293T cells were transiently transfected for 48 h with FLAG-D3Cys and Myc/His-tagged $\beta 3$/ $\beta 1$ integrin. The lysates were immunoprecipitated (IP) with FLAG-agarose beads and immunoblotted (IB) with the indicated antibodies; IgG was taken as a negative control. 1% of the lysate was loaded as input. Representative blot from three independent experiments is shown. (b) HEK-293T cells transiently transfected for 48 h with FLAG-D3Cys and Myc/His-tagged $\beta 3$ integrin for reverse pull down assay. Representative blot from three independent experiments is shown. The lysates were immunoprecipitated (IP) with FLAG-agarose beads and immunoblotted (IB) with the indicated antibodies; IgG was taken as a negative control. 1% of the lysate was loaded as input. (c) Schematic of a gold surface with $D3^{FL}$ protein immobilized on a sensor chip CM5 and associated protein ($\alpha v\beta 3$ integrin) over which buffer is flown was used as an analyte either alone or with inhibitors, in surface plasmon resonance (SPR) assay. (d) Sensorgrams depicting interaction of $D3^{FL}$ and $\alpha v\beta 3$ integrin in the absence of metal ions (inactive form of $\alpha v\beta 3$ integrin in varying concentrations). The average K_D values and the rate constants (ka and kd) were determined from at least two independent experiments. (e) Same as d except the buffer contained a combination of divalent cations, Mg^{2+}/Mn^{2+} (active form of $\alpha v\beta 3$ integrin in varying concentrations). (f) Same as e except that 100 nM of $\alpha v\beta 3$ active integrin was pre-incubated with cRGD (15 μM) or cRGD was used alone as an analyte without $\alpha v\beta 3$ integrin. (g) Same as e except that varying concentrations of active $\alpha v\beta 3$ integrin were pre-incubated with a combination of cRGD and Tetrac (15 μM each) and was used as an analyte. (h) HEK-293T cells transiently transfected for 48 h with FLAG-D3Cys and Myc/His-tagged $\beta 3$ integrin alone or in the presence of combination of 15 μM each cRGD peptide and Tetrac. The lysates were immunoprecipitated (IP) with FLAG-agarose beads and immunoblotted (IB) with the indicated antibodies; IgG was taken as a negative control. 1% of the lysate was loaded as input. Representative blot from three independent experiments is shown. Quantification of the band intensities as obtained is shown below as fold reduction. (i) Confocal micrographs obtained in Proximity ligation assay (PLA) depicting interaction between D3 and $\alpha v\beta 3$ as shown in arrows in each case as orange punctae-like fluorescence in the human kidney biopsies from healthy and patients with indicated glomerular diseases. Signal obtained from the normal IgGs as control is also shown in each case on the left side. Scale bar=50 μm.

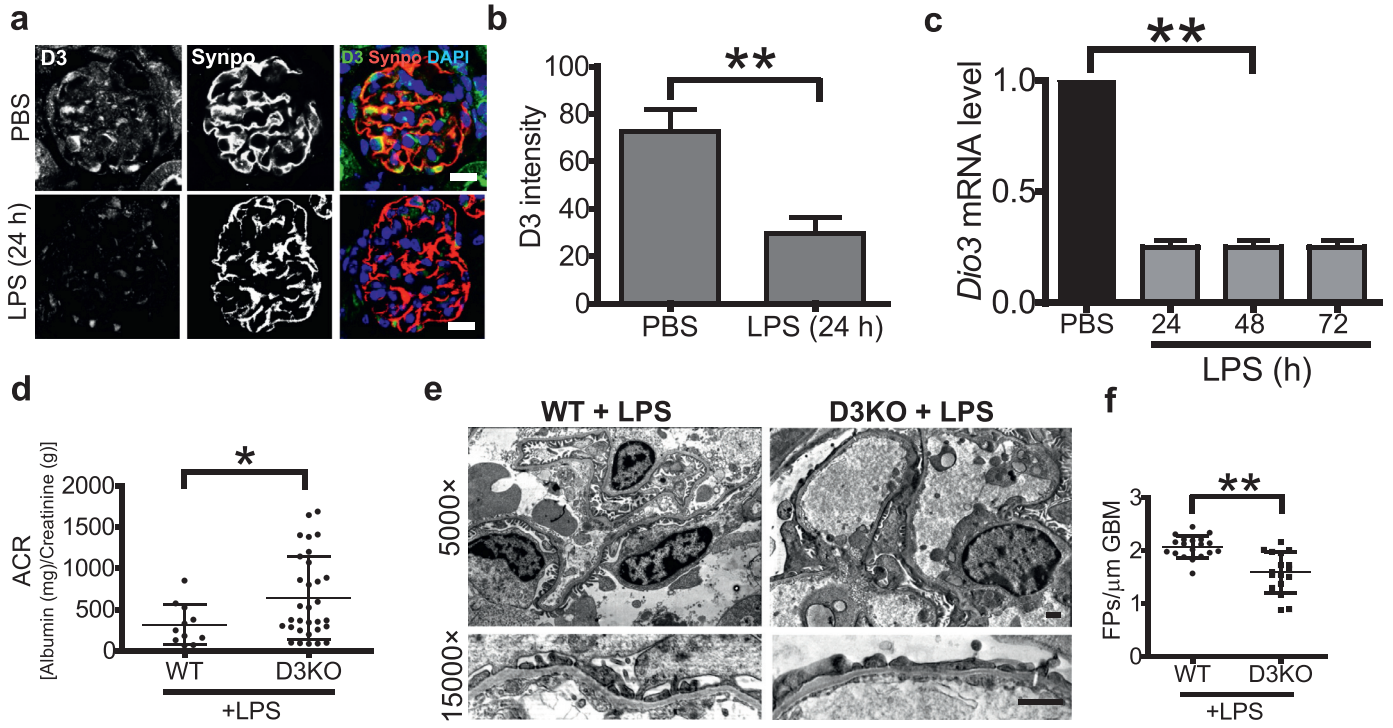

Fig. 4. LPS induced proteinuria is more severe in podocyte-specific D3 knockout mice (D3KO). (a) Confocal micrographs of 10-week-old mouse kidney showing decreased expression of D3 in glomeruli 24 h post LPS injection (10 mg/kg), identified by Synaptopodin stain. Left column, grayscale of α-D3; middle column, grayscale of α-Synaptopodin; right column, merge of α-D3 in green, α-Synaptopodin in red, DAPI in blue. Bar=10 μm. (b) Quantification of glomerular D3 intensity, Non-parametric two-tailed Students *t*-test was used to calculate the significance, $^{**}p \leq 0.01$. (c) qPCR analysis of *DIO3* mRNA expression in isolated glomeruli from mice treated with LPS at for indicated time points, Non-parametric two-tailed Students *t*-test was used to calculate the significance, $^{**}p \leq 0.01$. (d) Graph depicting Albumin (mg): Creatinine (g) ratio (ACR) measured from urine of 10-week-old D3KO mice ($n=31$) or littermate controls ($n=11$) 24 h post intraperitoneal (i.p) injection of LPS (5 mg/kg), Non-parametric two-tailed Students *t*-test was used to calculate the significance, $^{*}p \leq 0.05$. (e) Representative TEM micrographs of glomerular capillary loops of mice 24 h post LPS injection imaged at 5000 × and 15,000 × magnifications. FP effacement is shown in arrows. (f) FP effacement was quantified by counting the number of FPs per μm GBM in each of the samples, Non-parametric two-tailed Students *t*-test was used to calculate the significance, $^{**}p \leq 0.01$.

mRNA levels after 24 or 72 h of LPS treatment, as compared to the vehicle treated mice (Fig. 4c).

3.7. Podocyte-specific D3 knockout (D3KO) mice display severe foot process effacement and proteinuria

Our data clearly show that *Dio3* transcript levels, protein expression levels and D3 enzymatic activity decrease in mouse podocytes when exposed to an external assault. This suggests that reduced D3 levels correlate with a diseased phenotype and that its absence may have an adverse impact on glomerular filtration functions carried out by podocytes in kidney tissues. However, to test this hypothesis and to directly gauge the contribution of D3 to podocyte integrity, we generated a podocyte-specific D3 knockout (D3KO) mouse model (Supplementary Fig. 3).

Proteinuria, determined by establishing the albumin to creatinine ratio (ACR), was measured in both control and D3KO mice after treatment with a low dose of LPS to induce kidney damage. Elevated ACR was observed in LPS-treated D3KO mice as compared to the LPS-treated WT mice, indicating that the absence of D3 expression on podocytes leads to an increased susceptibility for the development of kidney disease (Fig. 4d). The glomerular capillary loops of LPS-treated WT control and D3KO mice were visualized using transmission electron microscopy (TEM). While the control group showed mild loss of podocyte foot processes (FPs) following LPS treatment, the D3KO group exhibited distinct FP effacement (Fig. 4e). Quantification of the FPs demonstrated a marked reduction in the number of FPs in the latter case (Fig. 4f).

Finally, to ascertain if inhibition of deiodinases globally would impact the podocytes locally, we used iopanoic acid (IOP), which is a potent pan-deiodinase inhibitor [32], and examined podocyte morphology. Ultrastructural analysis of the glomerular capillary loops from IOP-treated mice using TEM in combination with image quantification indeed showed a significant reduction in the number of FPs and profound effacement, when compared to the vehicle-treated control mice (Supplementary Fig. 4). While IOP also inhibits other deiodinases unbiasedly, we are confident that the effects observed are mediated via D3 inhibition given that the expression of D1 and D2 in podocytes is negligible.

3.8. Podocytes express TSH receptor (TSH-R) and its activation causes podocyte injury

A common association of nephrotic syndrome (NS) with thyroid malfunction is seen in Graves' disease, which is an autoimmune disorder caused by circulating autoantibodies against TSH-R, leading to overproduction of thyroid hormones. Therefore, we wanted to investigate if podocytes express TSH-R and if so, were they susceptible to anti-TSH-R antibody-mediated injury. Notably, our qPCR data revealed expression of *Tshr* mRNA in mouse podocytes, albeit lesser than what was observed in mouse thyroid (Fig. 5a). Further, immunoblotting of lysates from mouse podocytes and mouse thyroid tissue (used as a positive control), with anti-TSH-R antibody identified the presence of TSH-R in both glycosylated (holoreceptor, >100 kDa) and non-glycosylated (84 kDa) forms; whilst no bands were detected in K562 cell lysate, taken as a negative control (Fig. 5b). Additionally, we also performed flow cytometry to validate TSH-R expression on cultured mouse podocytes. A clear shift was observed for the FITC signal on the X-axis along with a ~2-fold increase in the mean fluorescence intensity (MFI) when podocytes were incubated with FITC-

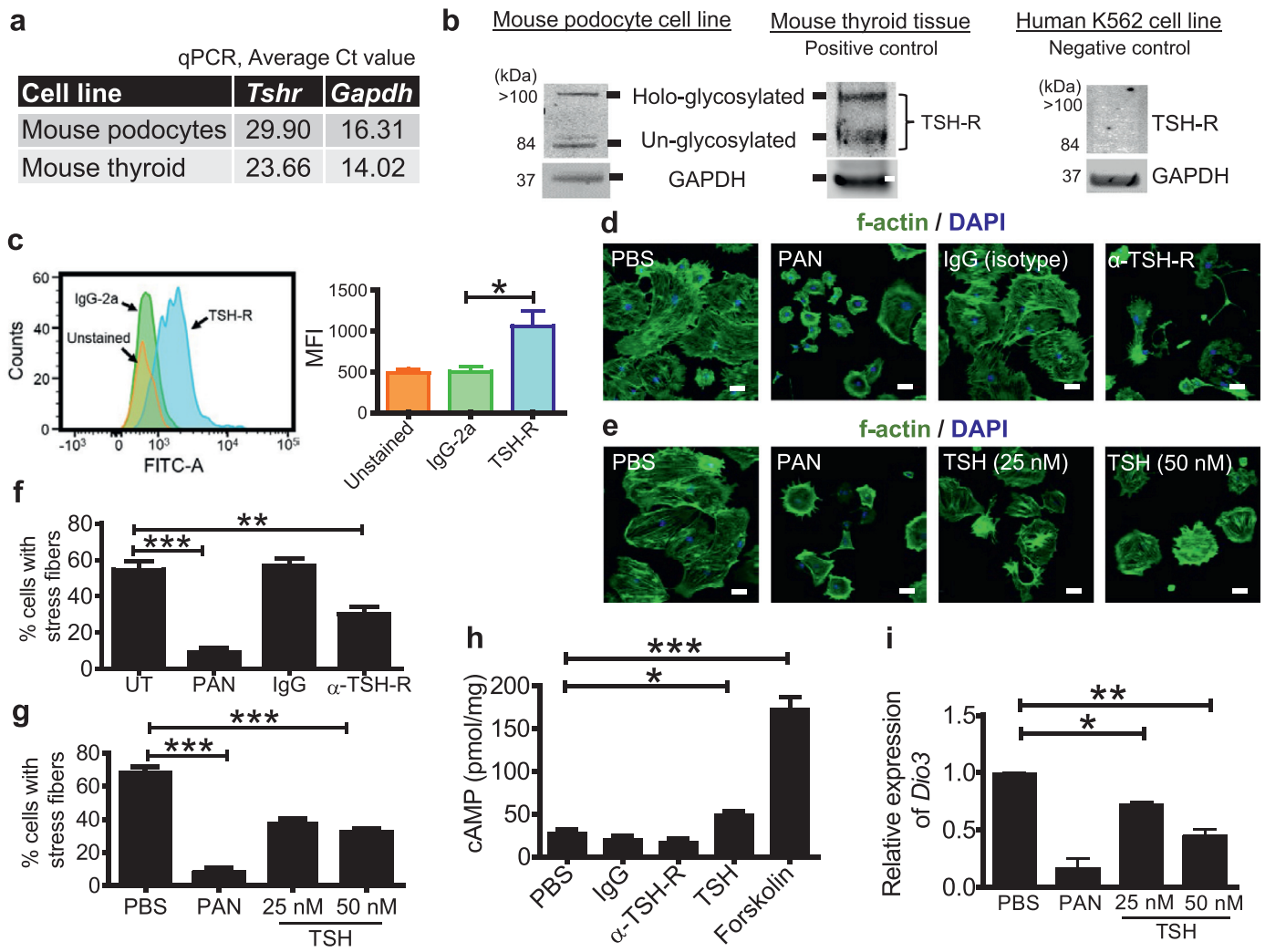

Fig. 5. Activation of TSH-R on podocytes is detrimental. (a) qPCR data showing the average Ct value from 2 independent wells for *tshr* gene in mouse podocytes and mouse thyroid in comparison to the housekeeping gene *gapdh*. (b) Western blot analysis of lysates from mouse podocytes, mouse thyroid tissue (positive control) and human K562 cells (negative control) probed with the indicated antibodies. Representative blot from two independent experiments is shown. Migration of molecular weight standards is depicted on the left as kDa. (c) Histogram depicting the data from flow cytometric analysis performed on mouse podocytes with FITC-conjugated TSH-R antibody (blue) overlapped with the controls (unstained, red and FITC-conjugated IgG2a isotype control, green). 5000 events were collected and gated. Graph on the right shows the geometric mean fluorescence intensity (MFI) on Y-axis obtained from four independent experiments. Non-parametric two-tailed Students *t*-test was used to calculate the significance, $^{*}p \leq 0.05$. (d) Confocal micrographs of cultured mouse podocytes left untreated (UT), PAN treated (30 μg/ml), Normal rabbit IgG isotype or anti-TSH-R antibody (3 μg/ml each) for 24 h. Stains: merge of F-actin phalloidin-488 stained in green and DAPI in blue. Scale bar=20 μm. (e) Confocal micrographs of cultured mouse podocytes left untreated (UT), PAN treated (30 μg/ml), or TSH (25 and 50 nM) for 24 h. Stains: merge of F-actin phalloidin-488 in green and DAPI in blue. Scale bar=20 μm. (f) Quantification of the data in d, represented as percentage of cells with normal cell shape and size with transversal stress fibers. Non-parametric two-tailed Students *t*-test was used to calculate the significance, $^{**}p \leq 0.01$ and $^{***}p \leq 0.001$. (g) Quantification of the data in e, represented as percentage of cells with normal cell shape and size with transversal stress fibers. Non-parametric two-tailed Students *t*-test was used to calculate the significance, $^{***}p \leq 0.001$. (h) cAMP levels (in pmol/ml) normalized with the protein concentration (mg/ml), plotted as pmol/mg in the culture supernatants of mouse podocytes exposed to the indicated treatments for 60 min. Non-parametric two-tailed Students *t*-test was used to calculate the significance, $^{***}p \leq 0.001$ *and* $^{*}p \leq 0.05$. (i) qPCR analysis of *DIO3* transcript in mouse podocytes upon PAN (30 μg/ml) and TSH (25 and 50 nM) treatment for 24 h. *gapdh* was used as the housekeeping gene; $^{**}p \leq 0.01$ *and* $^{*}p \leq 0.05$ determined using non-parametric Students *t*-test.

conjugated TSH-R antibody, compared to the isotype control which overlapped with the unstained podocytes (Fig. 5c and inset). Although, the results clearly indicate expression of TSH-R, whether this receptor is functionally active on the surface of podocytes and if the engagement of TSH-R with its ligand can provoke downstream signaling in podocytes was yet to be ascertained.

Since it is known that the TSH-R, in addition to its natural ligand [thyroid stimulating hormone (TSH)], can also be activated by TSH-R autoantibodies found in patients with Graves' disease [33, 34], mouse podocytes were exposed to both TSH and anti-TSH-R antibody. We expected TSH-R antibody to function as a clinically relevant TSH-R agonist. Interestingly, upon stimulation of TSH-R either directly by TSH or indirectly by TSH-R antibody, there were clear signs of cellular injury. α-TSH-R- (Fig. 5d, f) or TSH- (Fig. 5e, g) treated mouse podocytes exhibited changes in cell shape, F-actin depolarization and reduction in cell size; akin to the morphological changes seen in PAN-induced injury (Fig. 1).

A known outcome of TSH-R activation is robust cAMP induction [35, 36]. Indeed, as shown in Fig. 5h, ~2-fold increase in the cAMP was observed in the culture supernatant of podocytes treated with TSH in comparison to the untreated podocytes. As anticipated, cAMP levels were substantially higher in mouse podocytes exposed to Forskolin, a known inducer of cAMP. Intriguingly enough, we did not observe cAMP induction in TSH-R treated podocytes, and the levels were comparable to the podocytes treated with a non-specific antibody (isotype control) or resting podocytes (Fig. 5h). Similarly, injury caused by TSH (Fig. 5i) but not TSH-R (data not shown) was accompanied by a reduction in the *Dio3* mRNA levels.

4. Discussion

There is strong precedence for a functional intersection between thyroid and kidney complications [37, 38]. Our data support a concept of podocytes being regulated by a cellular TH signaling pathway with implications in kidney diseases. The classical understanding of the primary role for D3 is to minimize TH signaling and possibly reduce cellular energy demands, especially during disease states. D3 is predominantly expressed during embryonic life, but it is also found in the placenta, where it is linked to limiting the transfer of maternal TH to the fetus [39–41]. Interestingly, fully differentiated podocytes of diabetics undergo a reversion to a state that more closely resembles the early embryonic kidney [42]. These "*fetal-like*" changes in diabetic podocytes (characterized by cytoskeletal rearrangement, increased expression of fetal/mesenchymal markers, de-differentiation, maladaptive cell cycle induction/arrest, and hypertrophy) were attributed to high D3 expression with low levels of T3 within the podocyte. Similarly, in most reported models of tissue disease or injury like inflammation, liver regeneration, cardiac hypertrophy and infarct, and cancer, D3 levels are generally found to be elevated [43–45]; presumably to impede or slow down cellular metabolism. However, our data showing elevated amounts of D3 in healthy podocytes and its reduction in diseased/injured podocytes is opposite of what one would anticipate; challenging the existing paradigm. We surmise that D3 regulation in podocytes is clearly distinct from other cell types. This is indeed substantiated by reduced *DIO3* mRNA levels in diseased human kidneys. Further, high D3 expression can also be found in healthy adult cells such as neurons and keratinocytes [24].

D3 is an integral plasma membrane protein that has been shown to rapidly undergo Clathrin-mediated endocytosis followed by accumulation in the early endosomes from where it recycles back to the plasma membrane; a phenomenon that is thought to facilitate its longer half-life (12 h) compared to the other short-lived isoforms, D1 and D2 [46]. The present data demonstrate that exposure to either PAN, LPS or T3 leads to cellular D3 redistribution in podocytes, i.e., accumulation of the enzyme in the Golgi apparatus and cell nucleus. These findings are reminiscent of the redistribution of D3 from the plasma membrane to the cell nucleus in hypoxic cultured neurons [47] and in the ischemic rat cerebral cortex [48]. One question that should be explored is if the redistribution of D3 in podocytes observed under stressful conditions involves internalization of D3, or truncation of the Golgi export to the plasma membrane and redirection of newly synthesized D3 to the cell nucleus. Studies performed in hypoxic neurons support the latter mechanism [47]. Nonetheless, D3 apparently joins the expanding list of podocyte cell membrane proteins that undergo changes in subcellular localization, like the crucial slit diaphragm protein Nephrin and several integrins [49]. It is not surprising that these important structural and regulatory proteins present on the cell membrane would require some sort of tight regulation to cope and contend with the rigorous flux of metabolites while the cell performs fundamental filtration functions.

Exactly why the subcellular distribution of D3 is so dramatically affected under stressful conditions, and what it would accomplish could be answered by considering that TH receptors are located in the cell nucleus and D3 relocation to the nucleus has been shown to limit TH signaling [47]. In fact, nuclear accumulation of D3 in response to PAN-induced injury did decrease the transcription of two T3-repsonsive genes (*Pgc-1α* and *Hr*); indicating that D3 translocation to the nucleus upon external injury provides podocytes with an adaptive compensatory mechanism that allows for a rapid, localized inactivation of T3, thereby reducing the T3-induced gene transcription. Our study thus illustrates how D3 safeguards podocytes from exhaustion and death by averting futile energy expenditure during gene transcription (Fig. 6).

The classical well-studied and characterized genomic actions of THs are carried out by the binding of T3 to high-affinity nuclear TH receptors (TRs), which recognize specific TH-response elements (TREs) on the target genes and activate or repress transcription in response to T3. However, there is evidence showing that TH induces non-genomic (extranuclear) events independent of TRs. Since our previous work has established the importance of integrin signaling on podocyte health, we hypothesized that T3 signaling could lead to the activation of $\alpha v\beta 3$ integrin, too much of which is known to result in podocyte damage. The present study indicates that the presence of D3 on the podocyte membrane also modulates this novel pathway of T3 signaling. We envisioned a model that functions in several interconnected ways: (a) D3 in the healthy podocyte cell membrane inactivates T3 to dampen TH signaling. (b) D3 could also mitigate T3-mediated signaling in healthy podocytes through the $\alpha v\beta 3$ integrin receptor by directly interacting with the $\alpha v\beta 3$ integrin receptor and interfering with its activation. However, the absence of D3 on the plasma membrane, as seen during injury or stress and when T3 levels are in excess, leads to enhanced T3-$\alpha v\beta 3$ integrin interaction and subsequent signaling through the $\alpha v\beta 3$ integrin receptor, culminating in podocytopathy. Having said that, we do acknowledge that the effects observed upon T3 addition on podocytes may not be solely due to the activation of $\alpha v\beta 3$ integrin-mediated non-genomic branch. It is certainly possible that the nuclear or genomic signaling, which is initiated upon T3 binding to the TR receptors in the nucleus, might have contributed to some of the observed T3 outcome.

TH-mediated induction of a proliferative signaling pathway in an otherwise differentiated podocyte is quite deleterious for its critical cellular functions. The ability of TH stimulated podocytes to migrate faster could eventually be translated into their inability to adhere properly to the GBM. Thus, we speculate that the enhanced motility of podocytes observed in our *in vitro* model of hyperthyroidism could lead to podocyte detachment (loss of number) in addition to podocyte effacement (structural and functional loss). It is expected that by preventing or reducing some of the events that increase podocyte mobility, it may be possible to prevent podocyte effacement and thus limit glomerular injury. Thus, although studying the pathways that affect podocyte physiology warrants comprehensive investigation, the knowledge gained from these investigations may prove fruitful for future therapeutic interventions.

In the entirety, our findings cogently demonstrate that TH feeds a metabolic input into $\alpha v\beta 3$ integrin on podocytes and that D3 acts as a thyrostat by providing a mechanism whereby TH-activated integrin signaling can be modulated to offer renoprotection to podocytes (Fig. 6). Our data support a model wherein D3 interferes with the binding of $\alpha v\beta 3$ integrin to T3. Under healthy conditions, high D3 levels not only keep local T3 levels low (checkpoint 1) but also occupy binding sites on the integrin receptor (checkpoint 2) and interfere with activation by T3. When D3 levels at the plasma membrane are reduced during periods of stress or injury, D3-$\alpha v\beta 3$ integrin coupling is alleviated. In this situation, the integrin receptor is free to bind T3, leading to the rapid onset of T3-mediated $\alpha v\beta 3$ integrin signaling pathway activation.

Finally, our study attempts to delineate the plausible mechanisms that lead to podocyte damage and NS in the hyperthyroidic Graves' disease, which is caused by an abnormal activation of the TSH-R. We demonstrate for the first time that podocytes express an active and functional TSH-R and its activation is detrimental to the podocytes. In support of our findings, there exists a plethora of evidence in favor of extra-thyroidal expression of TSH-R and the ubiquitous presence of this receptor is becoming widely known [50]. Remarkably, renal expression of two thyroid-specific genes, TSH-R and thyroglobulin (Tg) has been reported [51]. Further, Dutton *et al* had confirmed TSH-R expression in human renal tubular cells with a prominence in distal tubules and collecting ducts [52]. Thus, TSH-R clearly has other moonlighting functions to perform besides controlling thyroid hormone production. Indeed, it will be quite intriguing to explore the

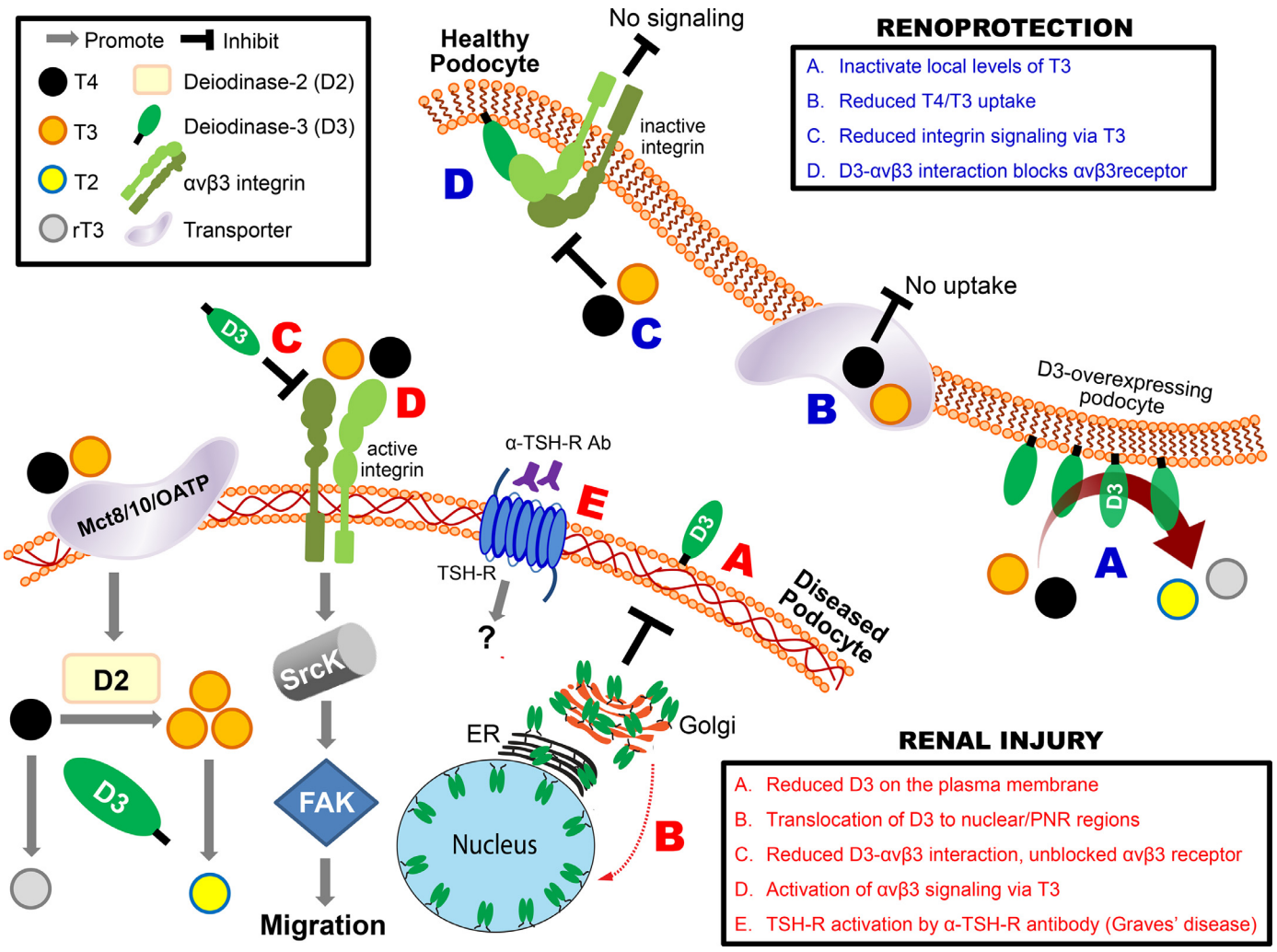

Fig. 6. A schematic illustrating the mechanism underlying the renoprotective role of D3 in podocytes. Under normal conditions, D3 is transcribed in the nucleus, translated/modified in the ER and Golgi, and is primarily trafficked to the plasma membrane (PM) of podocytes where it is highly expressed, and membrane bound. In response to injury, podocytes trigger an adaptive compensatory response which results in nuclear accumulation of D3. This allows for a rapid, localized deactivation of T3 in the nucleus where T3 receptors are abundant. In essence, due to the high energy demand of podocytes, we speculate that high levels of D3 activity is crucial to regulate energy homeostasis by dampening the cellular metabolism as a constructive process to promote energy conservation, thereby supporting essential functions that promote survival. However, the absence of D3 in injured podocytes leads to poor energy regulation and decreased ability to manage cellular stress, resulting in FP effacement, proteinuria, and glomerular disease. Another independent and parallel D3-mediated pathway leading to renoprotection in podocytes has been delineated. Interaction of D3 with $\alpha v\beta 3$ integrin functions as a second checkpoint to prevent activation of integrin-dependent pathways during hyperthyroidism. Further, over-expression of D3 reduces the systemic T3 levels and diminishes its cellular uptake. Therefore, D3 functions as a thyrostat on the surface of the podocytes; where its expression is finely tuned, both spatially and temporally, to offer renoprotection in a multi-pronged way. Presence of the TSH-R on podocyte surface and its activation following binding to TSH-R antibodies, as found in Graves' disease, presents an additional arm that contributes to podocyte damage via a cascade of unknown events; demonstrating another evidence in favor of thyroid-kidney synergy. Mct8: Monocarboxylate transporter 8 and 10; OATP: organic anion transporting polypeptide C1.

function and regulation of TSH-R in human kidneys, particularly in podocytes.

Signaling from the constitutively active TSH-R is augmented by its binding to TSH itself or by stimulating autoantibodies to the TSH-R. However, engagement of TSH-R by different ligands and different antibodies (stimulating, blocking or neutral) has been shown to contribute to thyroid pathology in a way that is quite distinct from its cognate ligand, TSH [53]. Thus, in the light of this, we can explain why activation of TSH-R by TSH resulted in a cAMP spike and a reduced *Dio3* transcript, but activation of the same receptor by TSH-R antibody yielded different results. From these illuminating observations, we can envisage that although both TSH-R-antibody and TSH induce podocyte injury at the morphological/structural level, they have a unique signaling imprint at the TSH-R. Further, cAMP induction is known to confer protection to podocytes against injury [54]. Interestingly, we observed that despite cAMP induction upon TSH-TSH-R engagement, podocytes underwent rounding and loss of actin cytoskeleton. Since our aim was to show that the TSH-R on podocytes is responsive to TSH and is thus functionally viable, we only looked at one aspect of TSH-TSH-R coupling, which is cAMP production. However, it is possible that the receptor-ligand engagement might have led to the parallel activation of other more dramatic pathological pathways, which potentially outweighed the protective effects of cAMP. In support of our explanation, a recent study by Yang *et al* [55] demonstrates that TSH binding to extrathyroidal TSH-Rs exerts different cell type-specific effects [56, 57].

Nevertheless, to the best of our knowledge, this novel study is a step forward in unraveling one of the many missing links in the regulation of thyroid-kidney axis.

Contributors

NJT, CC, AB and JR conceptualized the study; NJT and JR secured the research funding, SA, NJT and KHK designed and executed

majority of the experiments; KHK carried out the SPR, analyzed and interpreted the data, prepared the figure and provided valuable suggestions; RRD performed the ACR ELISA; JPW did the UPLC; YRS helped in purification of the recombinant proteins at Northwestern University; CL and DS generated the Flox-D3 mouse; BS provided her expertise in performing animal experiments; MMA and SM supervised the research and provided intellectual inputs; SA drafted the original manuscript and with contributions from NJT, MMA, SM, AB and JR, reviewed, edited and prepared the final version. SA, KHK and NJT are the guarantors of this work and had full access to all the data. SA, KHK, NJT, AB and JR have verified the underlying data and take responsibility for the integrity and accuracy of the data analysis. Further, all authors have read and approved the final version of the manuscript.

Declaration of Competing Interest

Jochen Reiser has patents on novel strategies for kidney therapeutics and stands to gain royalties from their commercialization. He is the co-founder of Walden Biosciences (Cambridge, MA, USA), a biotechnology company in which he has financial interest, including stock. Antonio Bianco is a consultant for Synthonics, Allergan, Abbvie, and BLA Technology. Other authors have nothing to disclose and there are no competing or conflicting interests.

Acknowledgements

We thank all the laboratory members for helpful discussions. Funding support from American Thyroid Association (ATA) to NJT (ATA-2018-050.R1) is appreciated. Authors thank Dr. Dileep Varma (Department of Cell and Developmental Biology) at Northwestern University for providing the facility for generation of recombinant proteins for SPR.

Supplementary materials

Supplementary material associated with this article can be found, in the online version, at doi:10.1016/j.ebiom.2021.103617.

References

[1] Reiser J, Altintas MM. Podocytes. F1000Res 2016;5. doi: 10.12688/f1000research.7255.1.
[2] Imasawa T, Rossignol R. Podocyte energy metabolism and glomerular diseases. Int J Biochem Cell Biol 2013;45(9):2109–18 S1357-2725(13)00197-0 [pii] 10.1016/j.biocel.2013.06.013.
[3] Muller-Deile J, Schiffer M. The podocyte power-plant disaster and its contribution to glomerulopathy. Front Endocrinol (Lausanne) 2014;5:209. doi: 10.3389/fendo.2014.00209.
[4] Reiser J. Circulating permeability factor suPAR: from concept to discovery to clinic. Trans Am Clin Climatol Assoc 2013;124:133–8 https://www.ncbi.nlm.nih.gov/pubmed/23874017.
[5] Peeters RP, Visser TJ. Metabolism of Thyroid Hormone. 2000. https://doi.org/NBK285545 [bookaccession].
[6] Mariani LH, Berns JS. The renal manifestations of thyroid disease. J Am Soc Nephrol 2012;23(1):22–6 ASN.2010070766 [pii] 10.1681/ASN.2010070766.
[7] Basu G, Mohapatra A. Interactions between thyroid disorders and kidney disease. Indian J Endocrinol Metab 2012;16(2):204–13 IJEM-16-204 [pii]. doi: 10.4103/2230-8210.93737.
[8] Braunlich H. Postnatal development of kidney function in rats receiving thyroid hormones. Exp Clin Endocrinol 1984;83(3):243–50. doi: 10.1055/s-0029-1210336.
[9] Kaptein EM. Thyroid function in renal failure. Contrib Nephrol 1986;50:64–72 http://www.ncbi.nlm.nih.gov/entrez/query.fcgi?cmd=Retrieve&db=PubMed&dopt=Citation&list_uids=3100133.
[10] Weetman AP. Graves' disease. N Engl J Med 2000;343(17):1236–48. doi: 10.1056/NEJM200010263431707.
[11] Esteve Simo V, Fontsere N, Saurina A, Ramirez de Arellano M. [Graves disease, hypothyroidism, and minimal-change glomerulonephritis]. Nefrologia 2008;28(2):230–1 https://www.ncbi.nlm.nih.gov/pubmed/18454723.
[12] Hasnain W, Stillman IE, Bayliss GP. Minimal-change renal disease and Graves' disease: a case report and literature review. NDT Plus 2011;4(2):96–8. doi: 10.1093/ndtplus/sfq213.
[13] Chadha V, US Alon. Bilateral nephrectomy reverses hypothyroidism in congenital nephrotic syndrome. Pediatr Nephrol 1999;13(3):209–11. doi: 10.1007/s004670050594.
[14] Kohrle J. The selenoenzyme family of deiodinase isozymes controls local thyroid hormone availability. Rev Endocr Metab Disord 2000;1(1-2):49–58 http://www.ncbi.nlm.nih.gov/entrez/query.fcgi?cmd=Retrieve&db=PubMed&dopt=Citation&list_uids=11704992.
[15] Bianco AC, Dumitrescu A, Gereben B, Ribeiro MO, Fonseca TL, Fernandes GW, et al. Paradigms of Dynamic Control of Thyroid Hormone Signaling. Endocrine reviews 2019;40(4):1000–47. doi: 10.1210/er.2018-00275.
[16] Dentice M, Salvatore D. Deiodinases: the balance of thyroid hormone: local impact of thyroid hormone inactivation. J Endocrinol 2011;209(3):273–82 JOE-11-0002 [pii] 10.1530/JOE-11-0002.
[17] Hernandez A. Structure and function of the type 3 deiodinase gene. Thyroid : official journal of the American Thyroid Association 2005;15(8):865–74. doi: 10.1089/thy.2005.15.865.
[18] Hayek SS, Koh KH, Grams ME, Wei C, Ko YA, Li J, et al. A tripartite complex of suPAR, APOL1 risk variants and alphavbeta3 integrin on podocytes mediates chronic kidney disease. Nat Med;23(8):945-53. https://doi.org/nm.4362[pii] 10.1038/nm.4362.
[19] Mundel P, Reiser J, Zuniga Mejia Borja A, Pavenstadt H, Davidson GR, Kriz W, et al. Rearrangements of the cytoskeleton and cell contacts induce process formation during differentiation of conditionally immortalized mouse podocyte cell lines. Exp Cell Res 1997;236(1):248–58 S0014482797937393 [pii].
[20] Dentice M, Ambrosio R, Damiano V, Sibilio A, Luongo C, Guardiola O, et al. Intracellular inactivation of thyroid hormone is a survival mechanism for muscle stem cell proliferation and lineage progression. Cell Metab 2014;20(6):1038–48. doi: 10.1016/j.cmet.2014.10.009.
[21] Berry MJ, Banu L, Chen YY, Mandel SJ, Kieffer JD, Harney JW, et al. Recognition of UGA as a selenocysteine codon in type I deiodinase requires sequences in the 3′ untranslated region. Nature 1991;353(6341):273–6 10.1038/353273a0.
[22] Takemoto M, Asker N, Gerhardt H, Lundkvist A, Johansson BR, Saito Y, et al. A new method for large scale isolation of kidney glomeruli from mice. Am J Pathol 2002;161(3):799–805 S0002-9440(10)64239-3 [pii] 10.1016/S0002-9440(10)64239-3.
[23] Hahm E, Wei C, Fernandez I, Li J, Tardi NJ, Tracy M, et al. Bone marrow-derived immature myeloid cells are a main source of circulating suPAR contributing to proteinuric kidney disease. Nat Med 2017;23(1):100–6 nm.4242 [pii] 10.1038/nm.4242.
[24] Huang MP, Rodgers KA, O'Mara R, Mehta M, Abuzahra HS, Tannenbaum AD, et al. The thyroid hormone degrading type 3 deiodinase is the primary deiodinase active in murine epidermis. Thyroid : official journal of the American Thyroid Association 2011;21(11):1263–8. doi: 10.1089/thy.2011.0105.
[25] Lee HW, Khan SQ, Khaliqdina S, Altintas MM, Grahammer F, Zhao JL, et al. Absence of miR-146a in Podocytes Increases Risk of Diabetic Glomerulopathy via Up-regulation of ErbB4 and Notch-1. J Biol Chem 2017;292(2):732–47 M116.753822 [pii] 10.1074/jbc.M116.753822.
[26] Simonides WS, Mulcahey MA, Redout EM, Muller A, Zuidwijk MJ, Visser TJ, et al. Hypoxia-inducible factor induces local thyroid hormone inactivation during hypoxic-ischemic disease in rats. The Journal of clinical investigation 2008;118(3):975–83. doi: 10.1172/JCI32824.
[27] Bergh JJ, Lin HY, Lansing L, Mohamed SN, Davis FB, Mousa S, et al. Integrin alphaVbeta3 contains a cell surface receptor site for thyroid hormone that is linked to activation of mitogen-activated protein kinase and induction of angiogenesis. Endocrinology 2005;146(7):2864–71 en.2005-0102 [pii] 10.1210/en.2005-0102.
[28] Davis PJ, Davis FB, Mousa SA, Luidens MK, Lin HY. Membrane receptor for thyroid hormone: physiologic and pharmacologic implications. Annu Rev Pharmacol Toxicol 2011;51:99–115. doi: 10.1146/annurev-pharmtox-010510-100512.
[29] Reiser J, Oh J, Shirato I, Asanuma K, Hug A, Mundel TM, et al. Podocyte migration during nephrotic syndrome requires a coordinated interplay between cathepsin L and alpha3 integrin. J Biol Chem 2004;279(33):34827–32. doi: 10.1074/jbc.M401973200.
[30] Shinderman-Maman E, Cohen K, Weingarten C, Nabriski D, Twito O, Baraf L, et al. The thyroid hormone-alphavbeta3 integrin axis in ovarian cancer: regulation of gene transcription and MAPK-dependent proliferation. Oncogene 2016;35(15):1977–87. doi: 10.1038/onc.2015.262.
[31] Wei C, El Hindi S, Li J, Fornoni A, Goes N, Sageshima J, et al. Circulating urokinase receptor as a cause of focal segmental glomerulosclerosis. Nat Med 2011;17(8):952–60. doi: 10.1038/nm.2411.
[32] Ramos-Dias JC, Lengyel AM. Iopanoic acid-induced decrease of circulating T3 causes a significant increase in GH responsiveness to GH releasing hormone in thyrotoxic patients. Clin Endocrinol (Oxf) 1999;51(4):461–7. doi: 10.1046/j.1365-2265.1999.00822.x.
[33] Ginsberg J, Shewring G, Smith BR. TSH receptor binding and thyroid stimulation by sera from patients with Graves' disease. Clin Endocrinol (Oxf) 1983;19(3):305–11. doi: 10.1111/j.1365-2265.1983.tb00003.x.
[34] Libert F, Lefort A, Gerard C, Parmentier M, Perret J, Ludgate M, et al. Cloning, sequencing and expression of the human thyrotropin (TSH) receptor: evidence for binding of autoantibodies. Biochem Biophys Res Commun 1989;165(3):1250–5. doi: 10.1016/0006-291x(89)92736-8.
[35] Boutin A, Krieger CC, Marcus-Samuels B, Klubo-Gwiezdzinska J, Neumann S, Gershengorn MC. TSH Receptor Homodimerization in Regulation of cAMP Production in Human Thyrocytes in vitro. Front Endocrinol (Lausanne) 2020;11:276. doi: 10.3389/fendo.2020.00276.
[36] Neumann S, Geras-Raaka E, Marcus-Samuels B, Gershengorn MC. Persistent cAMP signaling by thyrotropin (TSH) receptors is not dependent on internalization. FASEB J 2010;24(10):3992–9. doi: 10.1096/fj.10-161745.

[37] Chonchol M, Lippi G, Salvagno G, Zoppini G, Muggeo M, Targher G. Prevalence of subclinical hypothyroidism in patients with chronic kidney disease. Clin J Am Soc Nephrol 2008;3(5):1296–300 CJN.00800208 [pii] 10.2215/CJN.00800208.
[38] Iglesias P, Diez JJ. Thyroid dysfunction and kidney disease. Eur J Endocrinol 2009;160(4):503–15 EJE-08-0837 [pii] 10.1530/EJE-08-0837.
[39] Galton VA, Hiebert A. The ontogeny of iodothyronine 5′-monodeiodinase activity in Rana catesbeiana tadpoles. Endocrinology 1988;122(2):640–5. doi: 10.1210/endo-122-2-640.
[40] Huang H, Marsh-Armstrong N, Brown DD. Metamorphosis is inhibited in transgenic Xenopus laevis tadpoles that overexpress type III deiodinase. Proc Natl Acad Sci U S A 1999;96(3):962–7 http://www.ncbi.nlm.nih.gov/entrez/query.fcgi?cmd=Retrieve&db=PubMed&dopt=Citation&list_uids=9927676.
[41] Berry DL, Rose CS, Remo BF, Brown DD. The expression pattern of thyroid hormone response genes in remodeling tadpole tissues defines distinct growth and resorption gene expression programs. Dev Biol 1998;203(1):24–35 S0012-1606(98)98975-8 [pii] 10.1006/dbio.1998.8975.
[42] Benedetti V, Lavecchia AM, Locatelli M, Brizi V, Corna D, Todeschini M, et al. Alteration of thyroid hormone signaling triggers the diabetes-induced pathological growth, remodeling, and dedifferentiation of podocytes. JCI Insight 2019;4(18) 130249 [pii] 10.1172/jci.insight.130249.
[43] Boelen A, Kwakkel J, Alkemade A, Renckens R, Kaptein E, Kuiper G, et al. Induction of type 3 deiodinase activity in inflammatory cells of mice with chronic local inflammation. Endocrinology 2005;146(12):5128–34. doi: 10.1210/en.2005-0608.
[44] Dentice M, Luongo C, Ambrosio R, Sibilio A, Casillo A, Iaccarino A, et al. beta-Catenin regulates deiodinase levels and thyroid hormone signaling in colon cancer cells. Gastroenterology 2012;143(4):1037–47. doi: 10.1053/j.gastro.2012.06.042.
[45] Kester MH, Toussaint MJ, Punt CA, Matondo R, Aarnio AM, Darras VM, et al. Large induction of type III deiodinase expression after partial hepatectomy in the regenerating mouse and rat liver. Endocrinology 2009;150(1):540–5. doi: 10.1210/en.2008-0344.
[46] Baqui M, Botero D, Gereben B, Curcio C, Harney JW, Salvatore D, et al. Human type 3 iodothyronine selenodeiodinase is located in the plasma membrane and undergoes rapid internalization to endosomes. J Biol Chem 2003;278(2):1206–11 M210266200 [pii]. doi: 10.1074/jbc.M210266200.
[47] Jo S, Kallo I, Bardoczi Z, Arrojo e Drigo R, Zeold A, Liposits Z, et al. Neuronal hypoxia induces Hsp40-mediated nuclear import of type 3 deiodinase as an adaptive mechanism to reduce cellular metabolism. The Journal of neuroscience : the official journal of the Society for Neuroscience 2012;32(25):8491–500. doi: 10.1523/JNEUROSCI.6514-11.2012.
[48] Freitas BC, Gereben B, Castillo M, Kallo I, Zeold A, Egri P, et al. Paracrine signaling by glial cell-derived triiodothyronine activates neuronal gene expression in the rodent brain and human cells. The Journal of clinical investigation 2010;120(6):2206–17. doi: 10.1172/JCI41977.
[49] Inoue K, Ishibe S. Podocyte endocytosis in the regulation of the glomerular filtration barrier. Am J Physiol Renal Physiol 2015;309(5):F398–405 ajprenal.00136.2015[pii] 10.1152/ajprenal.00136.2015.
[50] Davies TF, Editorial Latif R. TSH Receptor and Autoimmunity. Front Endocrinol (Lausanne) 2019;10:19. doi: 10.3389/fendo.2019.00019.
[51] Sellitti DF, Akamizu T, Doi SQ, Kim GH, Kariyil JT, Kopchik JJ, et al. Renal expression of two 'thyroid-specific' genes: thyrotropin receptor and thyroglobulin. Exp Nephrol 2000;8(4-5):235–43. doi: 10.1159/000020674.
[52] Dutton CM, Joba W, Spitzweg C, Heufelder AE, Bahn RS. Thyrotropin receptor expression in adrenal, kidney, and thymus. Thyroid : official journal of the American Thyroid Association 1997;7(6):879–84. doi: 10.1089/thy.1997.7.879.
[53] Morshed SA, Latif R, Davies TF. Characterization of thyrotropin receptor antibody-induced signaling cascades. Endocrinology 2009;150(1):519–29. doi: 10.1210/en.2008-0878.
[54] Li X, Tao H, Xie K, Ni Z, Yan Y, Wei K, et al. cAMP signaling prevents podocyte apoptosis via activation of protein kinase A and mitochondrial fusion. PLoS One 2014;9(3):e92003. doi: 10.1371/journal.pone.0092003.
[55] Yang C, He Z, Zhang Q, Lu M, Zhao J, Chen W, et al. TSH Activates Macrophage Inflammation by G13- and G15-dependent Pathways. Endocrinology 2021;162(8). doi: 10.1210/endocr/bqab077.
[56] Klein JR. Physiological relevance of thyroid stimulating hormone and thyroid stimulating hormone receptor in tissues other than the thyroid. Autoimmunity 2003;36(6-7):417–21. doi: 10.1080/0891693031000160301 9.
[57] Zhang W, Tian LM, Han Y, Ma HY, Wang LC, Guo J, et al. Presence of thyrotropin receptor in hepatocytes: not a case of illegitimate transcription. J Cell Mol Med 2009;13(11-12):4636–42. doi: 10.1111/j.1582-4934.2008.00670.x.